8-2021

Development of A Highly Sensitive Pressure Sensing System with Custom-Built Software for Continuous Physiological Measurements

Masoud Panahi
Western Michigan University, masoudpan@gmail.com

DEVELOPMENT OF A HIGHLY SENSITIVE PRESSURE SENSING SYSTEM WITH CUSTOM-BUILT SOFTWARE FOR CONTINUOUS PHYSIOLOGICAL MEASUREMENTS

by
Masoud Panahi

A thesis submitted to the Graduate College
in partial fulfillment of the requirements
for the degree of Master of Science in Engineering
Electrical and Computer Engineering
Western Michigan University
August 2021

Thesis Committee:

Massood Z. Atashbar, Ph.D.,
Chair Bradley J. Bazuin, Ph.D.
Binu B. Narakathu, Ph.D.
Dinesh Maddipatla,Ph.D.

DEVELOPMENT OF A HIGHLY SENSITIVE PRESSURE SENSING SYSTEM WITH CUSTOM-BUILT SOFTWARE FOR CONTINUOUS PHYSIOLOGICAL MEASUREMENTS

Masoud Panahi, M.S.E.

Western Michigan University, 2021

In this work, a pressure sensing system was designed and fabricated by developing a highly sensitive cone-structured pressure sensor with a custom-built software for physiological monitoring applications. A novel highly sensitive cone structured porous polydimethylsiloxane (PDMS) based pressure sensor capable of detecting very low-pressure ranges was developed for respiration monitoring. The pressure sensor was fabricated using a master mold, a hybrid-structured dielectric layer, and fabric-based electrodes. The master mold with inverted cone structures was created using a rapid and precise three-dimensional (3D) printing technique. The dielectric layer, with pores and cone structures, was prepared by annealing a mixture of PDMS, nitric acid (HNO_3) and sodium bicarbonate ($NaHCO_3$) in a master mold with inverted cone structures. The electrodes were developed by screen printing silver functional ink on fabric. The porous-cone structures provided enhanced deformation and thus resulted in high sensitivity for detecting very low-pressure ranges below 100 Pa. As an application demonstration, the pressure sensor was sewed inside a surgical mask and its capability to detect different respiration rates (normal, fast, and deep breathes) was investigated. An airflow controller system and a custom-

built software was also developed for performing continuous sensor data acquisition and capacitance conversions for varying airflow rates.

ACKNOWLEDGMENTS

First and foremost, I wish to express my sincere gratitude to my supervisor and committee chair Dr. Massood Atashbar for his constant support and encouragement. He continuously guided me to become a better professional and always pushed me to make progress in my research projects. Dr. Atashbar always believes that it is his responsibility to train a good scientist engineer and I was able to do well with confidence because of his constant support. I am truly grateful to him for believing in me and providing many opportunities to improve myself.

My sincere thanks goes to the department chair and my committee member Dr. Bradley Bazuin for providing helpful suggestions and his valuable time in encouraging and supporting my thesis. I have been fortunate to have been guided by Dr. Binu Baby Narakathu and Dr. Dinesh Maddipatla throughout my master's thesis journey. Many brainstorming sessions with them made me gain a new learning experience. Every time I face challenges and problems and stumble a lot of questions, doubt, and fear of failing, their insights and ideas taught me to think in all possible dimensions and to come up with a solution.

Most importantly, none of this could have happened without my family. I wish to acknowledge the great love of my wife, also my colleague, Simin Masihi, for her constant support and encouragement. I am forever grateful to my parents Alireza Panahi and Tahereh Haji for their pure love. My special thanks to my little angel, Ariana Rose Panahi, who kept me going with her sweet smile.

Masoud Panahi

TABLE OF CONTENTS

Table of Contents - Continued

Table of Contents - Continued

LIST OF TABLES

LIST OF FIGURES

List of Figures - Continued

CHAPTER I

INTRODUCTION

1.1. Motivation

Wearable technology and health applications have recently gained a lot of momentum and are altering how patients access healthcare services. Wearable technology refers to a category of electronic devices that can be worn as accessories, embedded in clothing, implanted in the patient's body, or even tattooed on the skin [1-13]. These wearable devices can be used for continuous monitoring of various human physiological activities such as cardiac pulse, respiration rate, and body motions. Coronavirus disease (COVID-19) has spread globally since late 2019 and has affected the day-to-day life of millions of people worldwide. The outbreak of the COVID-19 crisis has significantly expanded the role of wearable technologies due to the critical need for remote monitoring services in the healthcare sector [14-26].

Highly sensitive pressure sensors, capable of being attached to the skin, fabric and clothing for continuous monitoring of diverse human physiological activities such as cardiac pulse, respiration rate, and body motions, have obtained an incredible research interests in recent years [27,28]. These pressure sensors have found a wide variety of applications specifically in wearable healthcare and patient rehabilitation center [28-30]. These pressure sensors should be highly responsive and detect pressures in range of 10 Pa in order to acquire/measure different physiological activity related information. The author has explored the development of a pressure sensing system consisting of highly sensitive wearable pressure sensors along with software and electronics to perform continuous monitoring of the human physiological activities.

1.2. Author's Contribution

My research work has resulted in 25 peer-reviewed journal and conference publications as well as two invention disclosures and patents (peer-reviewed journal publications (7), conference publications (21), intellectual property (IP) disclosures (1), patent publications (1)).

Journal Publications

1. S. Masihi, M. Panahi (granted with equal contribution as first author), D. Maddipatla, A. J. Hanson, A. K. Bose, S. Hajian, , V. Palaniappan, B. B. Narakathu, B. J. Bazuin, and M. Z. Atashbar, "A Highly Sensitive Porous PDMS Based Capacitive Pressure Sensor Fabricated on Fabric Platform for Wearable Applications," ACS Sensors Journal, https://dx.doi.org/10.1021/acssensors.0c02122, 2021. *(selected and featured in ACS Editors' Choice, an honor given to only one article from the entire ACS portfolio each day of the year. In addition, paper was selected as one of the TOP 10 MOST READ PAPERS IN APRIL 2021 at ACS Sensors). This work has also been reported in media for several times, such as:* https://www.azosensors.com/article.aspx?ArticleID=2224 *and* https://academictimes.com/flexible-sensors-could-pave-the-way-for-safer-sports-helmets/

2. V. Palaniappan, M. Panahi, D. Maddipatla, X. Zhang, S. Masihi, H. R. K. Manoj, B. B. Narakathu, B. J. Bazuin, M. Z. Atashbar, "Flexible M-Tooth Hybrid Micro-Structure Based Capacitive Pressure Sensors with High Sensitivity and Wide Sensing Range," IEEE Sensors Journal, 2021.

3. S. Masihi, M. Panahi, D. Maddipatla, A. K. Bose, X. Zhang, A. J. Hanson, B. B. Narakathu, B. J. Bazuin, and M. Z. Atashbar, "Development of a flexible tunable and compact microstrip

antenna via laser assisted patterning of copper film," IEEE Sensors Journal, vol. 20 (14), pp. 7579-7587, 2020.

4. V. Palaniappan, S. Masihi, M. Panahi, D. Maddipatla, A. K. Bose, X. Zhang, B. B. Narakathu, B. J. Bazuin, M. Z. Atashbar, "Laser-assisted fabrication of a highly sensitive and flexible micro pyramid-structured pressure sensor for E-Skin applications," IEEE Sensors Journal, vol. 20 (14), pp. 7605-7613, 2020.

5. A. K. Bose, X. Zhang, D. Maddipatla, S. Masihi, M. Panahi, B. B. Narakathu, B. J. Bazuin, J. D. Williams, M. F. Mitchell, M. Z. Atashbar, "Screen-printed strain gauge for micro-strain detection applications," IEEE Sensors Journal, vol. 20 (21), pp. 12652-12660, 2020.

6. S. Masihi, P. Rezaei, M. Panahi, "Compact chip-resistor loaded active integrated patch antenna for ISM band applications," Wireless Personal Communications, vol.97 (4), pp. 5733-5746, 2017.

7. S. Masihi, M. Panahi, D. Maddipatla, A. J. Hanson, S. Fenech, L. Bonek, N. Sapoznik, B. J. Bazuin, P. D. Fleming, and M. Z. Atashbar, "Development of a flexible wireless ECG monitoring device with dry fabric electrodes for wearable applications," IEEE Sensors Journal, 2021 (accepted).

Conference Publications

1. L. Bonek, S. Fenech, N. Sapoznik, A. J. Hanson, S. Masihi, D. Maddipatla, M. Panahi, and M. Z. Atashbar, "Development of a Flexible and Wireless ECG Monitoring Device," In 2020

IEEE Sensors, pp. 1-4. IEEE, 2020. *(selected as the first-place winner for the best student paper award)*

2. A. K. Bose, D. Maddipatla, X. Zhang, M. Panahi, S. Masihi, B. B. Narakathu, B. J. Bazuin, and M. Z. Atashbar, "Screen Printed Silver/Carbon Composite Strain Gauge on a TPU Platform for Wearable Applications," In 2020 IEEE International Conference on Flexible and Printable Sensors and Systems (FLEPS), pp. 1-5. IEEE, 2020.

3. X. Zhang, A. K. Bose, D. Maddipatla, S. Masihi, V. Palaniappan, M. Panahi, B. B. Narakathu, and M. Z. Atashbar, "Development of a Novel and Flexible MWCNT/PDMS Based Resistive Force Sensor," In 2020 IEEE International Conference on Flexible and Printable Sensors and Systems (FLEPS), pp. 1-4. IEEE, 2020.

4. S. Hajian, P. Khakbaz, B. B. Narakathu, S. Masihi, M. Panahi, D. Maddipatla, V. Palaniappan, R. G. Blair, B. J. Bazuin, and M. Z. Atashbar, "Humidity Sensing Properties of Halogenated Graphene: A Comparison of Fluorinated Graphene and Chlorinated Graphene," In 2020 IEEE International Conference on Flexible and Printable Sensors and Systems (FLEPS), pp. 1-4. IEEE, 2020.

5. V. Palaniappan, D. Maddipatla, M. Panahi, S. Masihi, A. K. Bose, X. Zhang, S. Hajian, B. B. Narakathu, B. J. Bazuin, and M. Z. Atashbar, "Highly Sensitive and Flexible M-Tooth Based Hybrid Micro-Structured Capacitive Pressure Sensor," In 2020 IEEE International Conference on Flexible and Printable Sensors and Systems (FLEPS), pp. 1-4. IEEE, 2020.

6. M. Panahi, S. Masihi, D. Maddipatla, A. K. Bose, S. Hajian, A. J. Hanson, V. Palaniappan, B. B. Narakathu, B. J. Bazuin, and M. Z. Atashbar, "Investigation of Temperature Effect on the Porosity of a Fabric Based Porous Capacitive Pressure Sensor," In 2020 IEEE International Conference on Flexible and Printable Sensors and Systems (FLEPS), pp. 1-4, 2020.

7. S. Hajian, B. B. Narakathu, D. Maddipatla, S. Masihi, M. Panahi, R. G. Blair, B. J. Bazuin, and M. Z. Atashbar, "Flexible Temperature Sensor based on Fluorinated Graphene," In 2020 IEEE International Conference on Electro Information Technology (EIT), pp. 597-600, 2020.

8. S. Masihi, M. Panahi, S. Hajian, D. Maddipatla, S. Ali, X. Zhang, A. K. Bose, B. B. Narakathu, B. J. Bazuin, and M. Z. Atashbar, "A Highly Sensitive Capacitive Based Dual-Axis Accelerometer for Wearable Applications," In 2020 IEEE International Conference on Electro Information Technology (EIT), pp. 557-561, 2020.

9. S. Masihi, M. Panahi, A. K. Bose, D. Maddipatla, A. J. Hanson, B. B. Narakathu, B. J. Bazuin, M. Z. Atashbar, "Rapid prototyping of a tunable and compact microstrip antenna by laser machining flexible copper tape," IEEE International Conference on Flexible and Printable Sensors and Systems (FLEPS), pp.1-3, 2019.

10. S. Masihi, M. Panahi, D. Maddipatla, A. K. Bose, X. Zhang, A. J. Hanson, V. Palaniappan, B. B. Narakathu, B. J. Bazuin, M. Z. Atashbar, "A novel printed fabric based porous capacitive pressure sensor for flexible electronic applications," IEEE SENSORS, pp.1-4, 2019. *(Selected as finalist for the IEEE SENSORS 2019 best student paper award)*

11. V. Palaniappan, S. Masihi, M. Panahi, D. Maddipatla, A. K. Bose, X. Zhang, B. B. Narakathu, B. J. Bazuin, M. Z. Atashbar, "Laser-assisted fabrication of flexible micro-structured pressure sensor for low pressure applications," IEEE International Conference on Flexible and Printable Sensors and Systems (FLEPS), pp. 1-3, 2019.

12. V. Palaniappan, S. Masihi, X. Zhang, S. Emamian, A. K. Bose, D. Maddipatla, S. Hajian, M. Panahi, B. B. Narakathu, B. J. Bazuin, M. Z. Atashbar, "A flexible triboelectric nanogenerator fabricated using laser-assisted patterning process," IEEE SENSORS, pp.1-4, 2019.

13. A. K. Bose, X. Zhang, D. Maddipatla, S. Masihi, M. Panahi, B. B. Narakathu, B. J. Bazuin, M. Z. Atashbar, "Highly sensitive screen-printed strain gauge for micro-strain detection," 2019 IEEE International Conference on Flexible and Printable Sensors and Systems (FLEPS), pp.1-3, 2019.

14. D. Maddipatla, X. Zhang, A. K. Bose, S. Masihi, M. Panahi, V. Palaniappan, B. B. Narakathu, B. J. Bazuin, M. Z. Atashbar, "Development of a flexible force sensor using additive print manufacturing process," 2019 IEEE International Conference on Flexible and Printable Sensors and Systems (FLEPS), pp. 1-3, 2019.

15. S. Masihi, P. Rezaei, M. Panahi, "Design of wideband microstrip antenna with spiral slot on ground plane," IEEE International Symposium on Antennas and Propagation & USNC/URSI National Radio Science Meeting, pp. 1934-1935, 2015.

16. S. Masihi, M. Panahi, D. Maddipatla, S. Hajian, A. K. Bose, V. Palaniappan, B. B. Narakathu, B. J. Bazuin, M. Z. Atashbar, “Cohesion failure analysis in a bi-layered copper/kapton structure for flexible hybrid electronic sensing applications,” Electro/information technology (EIT) Conference 2021, DOI: 10.1109/EIT51626.2021.9491906.

17. M. Panahi, S. Masihi, A. J. Hanson, D. Maddipatla, X. Zhang, V. Palaniappan, B. B. Narakathu, B. J. Bazuin, and M. Z. Atashbar, “Highly sensitive cone-structured porous pressure sensors for respiration monitoring applications,” In 2021 IEEE Sensors Conference, pp. 1-4, 2021.

18. Y. Beyene, R. Bahre, F. Mohammed, S. Masihi, A. Hanson, M. Panahi, D. Maddipatla, M. Z. Atashbar, “Development of a flexible wireless MWCNTs-based ECG monitoring device,” In 2021 IEEE Sensors Conference, pp. 1-4, 2021.

19. V Palaniappan, S Masihi, M Panahi, D Maddipatla, X Zhang, BB Narakathu, BJ Bazuin, MZ Atashbar, “A porous microstructured dielectric layer based pressure sensor for wearable applications,” 2021 IEEE International Conference on Flexible and Printable Sensors and Systems (FLEPS), pp. 1-4, 2021, DOI: 10.1109/FLEPS51544.2021.9469706.

20. A. J. Hanson, D. Maddipatla, A. K. Bose, C. J. Kosik, S. Hajian, M. Panahi, S. Masihi, B. B. Narakathu, B. J. Bazuin, M. Z. Atashbar, “Flexible and portable electrochemical system for the detection of analytes,” 2021 IEEE International Conference on Flexible and Printable Sensors and Systems (FLEPS), pp. 1-4, 2021, DOI: 10.1109/FLEPS51544.2021.9469822.

21. S. Hajian, S. M. Tabatabaei, B. B. Narakathu, D. Maddipatla, S. Masihi, M. Panahi, P. D. Fleming, B. J. Bazuin, M. Z. Atashbar, "Chlorine-terminated titanium carbide MXene as nitrogen oxide gas sensor: a first-principles study," 2021 IEEE International Conference on Flexible and Printable Sensors and Systems (FLEPS), pp. 1-4, DOI: 10.1109/FLEPS51544.2021.9469784.

Inventions: Patent Intellectual Property

1. M. Z. Atashbar, B. B. Narakathu, S. Masihi, M. Panahi, D. Maddipatla, "Pressure monitoring systems for helmet," Western Michigan University, U.S. Patent Application 16/898,588, filed December 17, 2020.

2. M. Z. Atashbar, S. Masihi, M. Panahi, D. Maddipatla, B. B. Narakathu, "Development of printed and flexible electrodes for wound healing and pain management application," Western Michigan University, Intellectual Property Disclosure, WMU Case #2020-002.

Awards

1. Graduate Student Research Grant (GSRG), Fall 2019, Western Michigan University

2. Department-Level Graduate Research and Creative Scholar Award (2020), Western Michigan University

3. Student Virtual Conference Grant (2020), Western Michigan University

1.3. Organization of Thesis

The rest of this thesis is divided into five chapters. In Chapter 2, the author presents a comprehensive literature review on different types of sensors and sensing mechanisms. This

review provides the basic introduction on various sensor classifications, followed by a background about wearable and highly sensitive pressure sensing technology along with the fabrication techniques, and health monitoring sensors. Chapter 2 provides an introduction to the sensor data acquisition techniques and requirements. In Chapter 3, the author provides a detailed discussion on a research project that involves the development of a flexible highly sensitive porous cone based capacitive pressure sensor. This includes explanation on the design, fabrication steps, and characterization of the capacitive porous pressure sensor, where a highly sensitive capacitive pressure sensor with dielectric layer made of pores and cone structures was fabricated to detect varying low pressures of the air flow during respiration. Chapter 4 presents the development of a software for a pressure sensing system and an airflow controller system, by implementing required algorithms and flowcharts. Finally, Chapter 5 summarizes this work.

CHAPTER II

LITERATURE REVIEW

2.1. Introduction

In this chapter, the author provides a literature review on different types of sensors and sensing mechanisms [31-72]. This chapter is divided into three sections followed by a summary. Section 2.2 provides an introductory discussion about sensors and their classifications, followed by an introduction to flexible hybrid electronics (FHE) features and requirements, and sensors for health monitoring [73-127]. Section 2.3 provides a review on pressure sensors, by introducing different types of pressure sensing transducers. In this section, the author introduces some of the wearable pressure sensors used for remote health monitoring by emphasizing the significance of cone-structured porous capacitive pressure sensing. Section 2.4 provides a review on sensor acquisition techniques and the need for software development in collecting big data sets, as an introductory requirement for extracting and analyzing the algorithms for machine learning purposes. In section 2.5 author provides a summary of this chapter.

2.2. Sensors

2.2.1. Introduction to Sensors

Nowadays, we live in a world of sensors. Various types of sensors can be found in our homes, offices, cars, and even in our clothes. The increasing use of sensors has significantly made our lives easier. For example, automating the adjustment of the room temperature, turning on the lights, detecting smoke or toxic gases, opening entrance doors as soon as we are near the door and many other tasks. In addition, the overwhelming growth of the sensor technology can make our lives healthier and probably longer in the future, by increasing the frequency of recording and monitoring health metrics. We can check our heart rate, blood sugar level, and oxygen saturation

rate at any time while doing the daily routines. This is due to a major change in the way patients access healthcare which has been realized by advances in wearable sensing technology and various health monitoring applications.

There are different, but similar, definitions for the word “sensor”. A sensor can be defined as an input device that provides an output in response to a specific physical quantity (input). From the definition of the sensor, it can be understood that the sensor named as “input device” is part of a more complex system which provides the input to a main control system such as a processor or a microcontroller. In the other words, a sensor can be defined as a device that can convert the input signals from different energy domains into electrical domain which can be understood by processors. The most familiar sensing system can be found in the human body. Human sensing system consists of different types of sensors that are capable of detecting different stimulus. This sensing system consists of sensory neurons, neural pathways, and parts of the brain involved in sensory perception. Commonly recognized sensory systems in the human body and most mammals are related to vision, hearing, touch, taste, and smell (Fig. 2.1) [128].

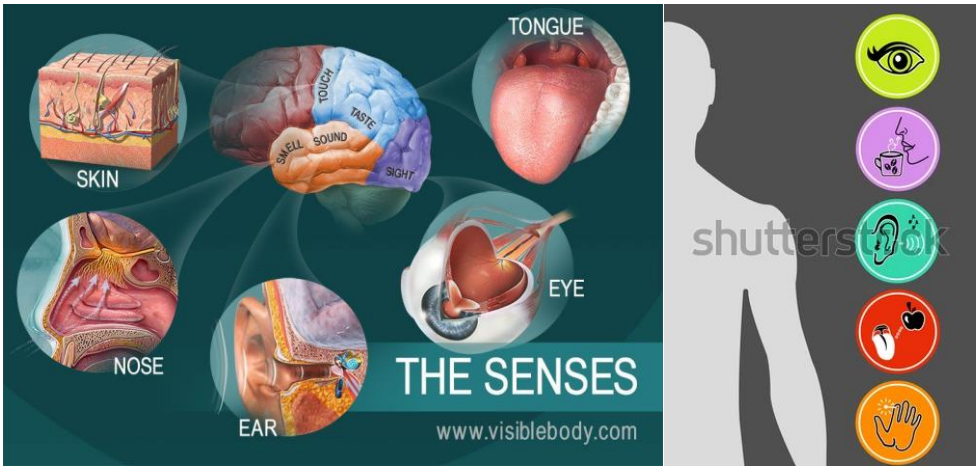

Figure 2.1. Human sensory system: The five senses.
[*Source:https://i.pinimg.com/originals/d7/4e/41/d74e41bd677aa29e578c5ea7c8813627.jpg*]

2.2.2. Classification of Sensors

The classification of sensors is based on the conversion phenomenon between the input and the output. Some of the common conversion phenomena are based on acoustic, photoelectric, thermoelectric, electrochemical, mechanical, and electromagnetic mechanisms. Table 2.1 shows different types of the sensors and their corresponding stimulus to which the conversion phenomenon occurs between the input and the output [129].

Table 2.1. Types of sensors and corresponding stimulus.

Sensor Type	Stimulus
Acoustic	Wave Amplitude, Phase or Velocity
Photoelectric	Light Reflection and Transmission
Thermoelectric	Temperature, Voltage
Electrochemical	Chemical or Biological Reaction
Electromagnetic	Electrical Current
Mechanical	Pressure, Force, Strain, Stress

2.2.3 Flexible Hybrid Electronics and Wearable Sensors

While flexible electronics have been around for years, either as flexible printed circuit boards (PCB) or printed electronics, there has always been a trade-off between flexibility and functionality [130]. However, flexible hybrid electronics (FHE) promises to combine the extensive processing capability of the integrated circuits with a flexible form factor, and printing processes rather than etched conductive interconnects [131,132]. Basically, the word hybrid in FHE means that this technology is the combination of printed electronics and silicon IC technology. This combination opens a wide range of application possibilities, across many

different industries. FHE technology utilizes both printed electronics and silicon IC's to develop electronics which can be flexible, stretchable, bendable, conformable, transparent, biocompatible, and light weight [131]. However, the interfacing of soft and hard electronics is a key challenge in field deployable demonstration of FHE devices and has become one of the important research areas [133]. Figure 2.2(a) shows the depiction of an FHE based circuit, printed onto a flexible substrate along with an integrated circuit. Additional functionalities such as thin film photovoltaics (PV), a thin film battery and printed sensors can also be included.

A market forecast of the total revenue from FHE over the next 10 years is shown in Fig. 2.2(b) and is divided into major categories [133]. Each category is made up of multiple forecast subcategories and components. while wearable/healthcare applications (especially skin patches) will dominate over the next 5 years, smart packaging will ultimately become the largest application. The FHE market shows a compound annual growth rate (CAGR) of 16.2% from 2020 to 2026. However, the market is still in its infancy, with a very limited number of manufacturers that have commercialized their products. The majority of the players developing this technology are in their R&D phase. In addition, due to the outbreak of COVID-19, there has been a disruption in the electronics industry's supply chain which is challenging the market growth. However, it is worth noting that the COVID-19 crisis has expanded the role of wearable technologies in the healthcare sector due to the need for remote monitoring services.

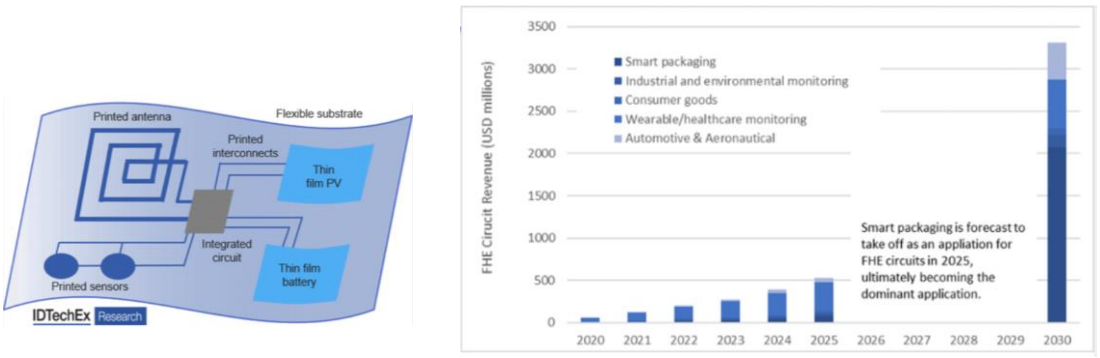

(a) (b)

Figure 2. 2. (a) Flexible hybrid electronics circuit and (b) market forecast (by revenue) for the adoption of FHE for various applications. *[Source: https://agilitypr.news/Flexible-Hybrid-Electronics-New-IDTechE-9650]*

Wearable electronics refer to textiles and clothing with integrated electronic technology or other computing devices that provide smart functionalities and relies on sensors to measure health metrics and various other parameters of the human body, and provides the consumers with data

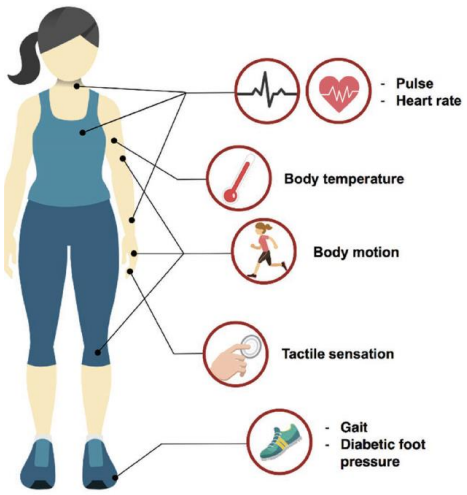

Figure 2.3. Different types of wearable sensors.

about themselves. After the smart phone revolution, it is now the wearable technology that will revolutionize how we wear smart devices on the body. Different products are being offered in the form of health monitors, gaming wears, clothing, security wears, fitness, and even jewelry to meet

various costumer needs. Figure 2.3 shows examples of different types of wearable sensors that can be used on the human body. FHE has the capability to further progress the field of wearable electronics by improving conformability along with functionality.

2.2.4. Sensors for Health Monitoring

Depending upon the measuring parameters, health monitoring sensors can be categorized into two major types: electrical sensors and non-electrical sensors. Electrical sensors can derive electrical signals such as electrocardiogram (ECG), electroencephalography (EEG), and electromyography (EMG) whereas non-electrical sensors can derive other physical and chemical signals. Some of these health monitoring sensors [14,134] include pulse oximeters, sweat sensors, temperature sensors, glucose sensors and accelerometers, are discussed below:

- Pulse oximeters measure oxygen saturation in blood and pulse rate. It employs the use of spectral analysis or spectrometry for measuring the ratio of oxy-haemoglobin and haemoglobin. Spectrometry is dependent on the distance that the light travels through a substance and because of different absorption levels will be emitted at different wavelengths.
- Sweat sensors use humidity sensors on a textile substance. The diffusion flow can be calculated using the difference in the humidity level. Alternatively, sweat sensors that use conductivity value for measuring the sweat rate in human body have also been utilized.
- Temperature sensors are used to measure body temperature at different situations such as normal body temperature, before or after surgery, during illness, etc. Micro-thermistors or thermocouples may also be used to measure temperature.

- Glucose sensors are the earliest developed bio-sensors which can measure metabolism of human body [134]. The highly selective and sensitive electro-chemical glucose sensors are used to measure glucose concentration in human body via colorimetry, fluorescence. The most recent glucose sensors work based on the enzymatic glucose reactions in human body.
- Accelerometer sensors are used to detect motion, velocity, tilt, position and fall based on the angular velocity and piezoelectric effect. The recent tri-axial accelerometer sensor can measure the position of the human body in three dimensions. Rotatory transducers are also used to measure the multi-position of human body.

Wearable devices have been intensively developed to be integrated with health monitoring systems as they provide essential features such as real-time monitoring, abnormalities detection, lower cost, minimum power consumption and health awareness. Some examples of wearable devices include a vest for monitoring vital parameters; smart shirt that measures ECG signals; and electronic patch and photodiode as pulse oximetry sensors [14].

2.3. Pressure Sensors

The sensing mechanisms of pressure sensors can be classified as piezoelectric, piezoresistive, and capacitive. Among these transduction mechanisms, capacitive pressure sensors with an enhanced sensitivity are good candidates for covering a wide range of sensitivity, desired in different applications. Over the past years, pressure sensors have been typically fabricated using conventional silicon manufacturing technologies. However, the conventional methods lack flexibility, with complex and expensive fabrication process.

2.3.1. Piezoelectric Mechanism

Piezoelectric sensors convert mechanical energy (either force, pressure, strain, vibration, etc.) into an electrical signal or vice versa. The most common sensing material used in the fabrication

of piezoelectric sensors is a perovskite ceramic material (lead zirconate titanate (PZT)) as shown in Fig. 2.4 [135]. Piezoelectric sensors are among the most demanding sensors which can be used in medical applications, and self-powered energy harvesting sensors. Recently, researchers have developed the next-generation piezoelectric sensors which are highly efficient, durable, lightweight and can be used as self-power sensors [136].

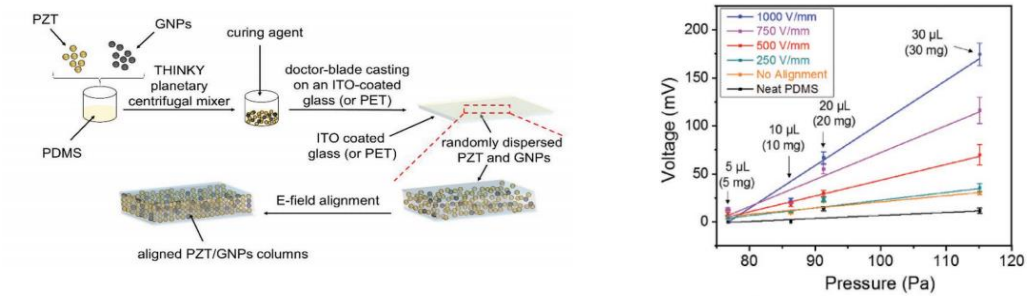

(a) (b)

Figure 2.4. (a) A novel fabrication process to produce ultrasensitive, flexible, and transparent piezoelectric materials using both lead zirconate titanate nanoparticles, and graphene nanoplatelets (b) The output voltage of PZT/PDMS samples aligned at different field strengths as a function of various water drop pressures [135]. *[Source: A. Yildirim, R. Rahimi, S. S. Es-haghi, A. Vadlamani, F. Peng, M. Oscai, and M. Cakma, "Roll-to-Roll (R2R) production of ultrasensitive, flexible, and transparent pressure sensors based on vertically aligned lead zirconate titanate and graphene nanoplatelets," Adv.Mater. Technol., vol. 4 (3), pp. 1800425, 2019]*

2.3.2. Piezoresistive Mechanism

Piezoresistive strain gauges are among the most common types of pressure sensors. Piezoresistive pressure sensors measure the pressure based on the change in the electrical resistance of a material when stretched. These pressure sensors are suitable for a variety of applications because of their simplicity of fabrication and durability. They can be used for measuring absolute, gauge, relative and differential pressure in different applications by covering both high and low pressure ranges. The working mechanism of the piezoresistive pressure sensor is to use a conductive strain gauge that its electrical resistance changes when it is stretched. The change in resistance is converted to an output signal. For example, the strain gauge can be attached to a diaphragm and recognize a change in resistance when the sensor element is deformed. There

are three main effects that can contribute to a change in the resistance of a conductive material. These effects include the conductor length (stretching increases the resistance), its cross-sectional area (to which the resistance is inversely proportional), and the inherent resistivity of some materials that can change when it is stretched. The piezoresistive effect and sensitivity is specified by the gauge factor, which is defined as the relative resistance change divided by the strain, and varies greatly between materials. Strain gauge elements can be made of metal or a semiconducting material. The resistance change in metal strain gauges is mainly the result of the change in sensors' geometry (length and cross-sectional area). In some metals such as platinum alloys, the piezoresistive effect can increase the sensitivity by a factor of two or more [137,138].

2.3.3. Capacitive Mechanism

Among all the pressure sensing mechanisms, capacitive pressure sensors are reported to provide excellent sensitivity, relatively shorter response time and long-term stability with low power consumption [139-143]. Typically, the capacitive pressure sensors consist of a dielectric layer sandwiched between two conductive electrodes (top and bottom electrodes) as shown in Fig. 2.5. Capacitive based pressure sensors in principle are parallel plate capacitors and its capacitance can be calculated using Eq. (1),

$$C_0 = \frac{\varepsilon_0 \varepsilon_r A}{d} \qquad (1)$$

where C_0, $\mathcal{E}_0$, $\mathcal{E}_r$, A, and d are the base capacitance, the permittivity of the free space, the relative permittivity of the dielectric layer, sensor contact area, and the thickness of the dielectric layer, respectively. The capacitance is directly proportional to the dielectric constant and the overlap area of the two plates, and is inversely proportional to the thickness of the dielectric layer which determines the distance between the two electrodes. By increasing the overlapping area and dielectric constant, or decreasing the plates' distance, the capacitance can be increased. When an

external force is applied to the sensor, the dielectric layer deforms and the distance between the two electrodes of the capacitive pressure sensor decreases accordingly and causes an increase in the capacitance. As the deformation of the dielectric layer increases, the pressure sensor gets more compressed and provides higher output capacitance change, resulting in increased sensitivity.

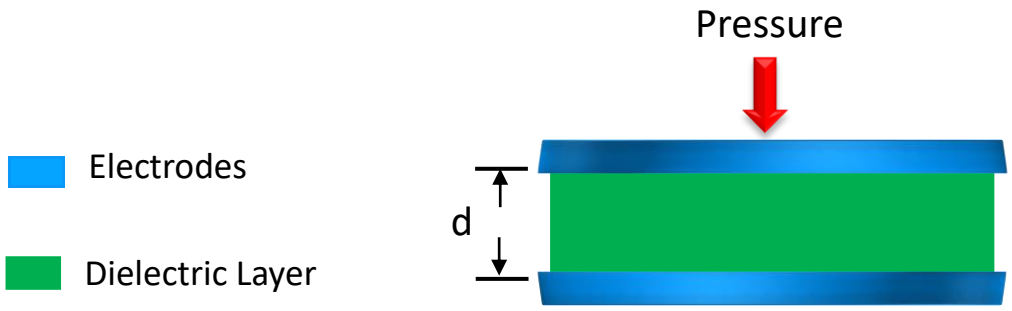

Figure 2.5. Capacitive pressure sensors consisting of a dielectric layer sandwiched between two conductive electrodes (top and bottom electrodes).

2.3.4. Structured Capacitive Pressure Sensors

In recent years, constant efforts have been made to increase the sensitivity of the pressure sensors by reducing the elastic modulus of the elastomeric dielectric layer and thus increasing its deformation. Silicone based elastomeric polymers such as polydimethylsiloxane (PDMS) have been extensively employed as a dielectric layer in the fabrication of capacitive based pressure sensors, since PDMS provides excellent mechanical strength, flexibility, stretchability and conformability [144]. Several attempts have been reported to increase the sensitivity of PDMS based pressure sensors by modifying the dielectric layer properties to increase its deformation under the application of an external pressure. Micro-structured dielectric layers are reported to have a significant effect in increasing the deformation of the dielectric layer by reducing the elastic modulus of the elastomeric dielectric layer. As the deformation of PDMS increases, the

pressure sensor gets more compressed and provides higher output capacitance change, resulting in an increased sensitivity. The common fabrication techniques for developing micro-structured dielectric layers include:

- Three dimensional (3D) sacrificial templates such as sugar or salt
- Micro-patterning techniques such as laser patterning
- Emulsions of oil aqueous solutions obtained by mixing water and PDMS
- Nanomaterial fillers such as carbon particles
- Developing water droplets or gas packets by injecting water or realizing gas

In all the aforementioned fabrication techniques, creating the micro-pores/structures in the elastomeric dielectric layer causes a significant decrease in the elastic modulus which in turn increases the deformation and thus the sensitivity of the fabricated capacitive pressure sensors. Figure 2.6 shows micro-structured dielectric layers using different fabrication techniques. pressure sensors by micro-structuring the dielectric layer material, there is no research available on the development of pressure sensors with dielectric layers made of hybrid microstructures (combined two or more microstructures). It is envisioned that the pressure sensors developed with hybrid micro-structured dielectric layers will result in ultra-high sensitivity sensors for respiration rate monitoring applications [143]. J. C. Yang et al. [144] have reported an ultra-high sensitive capacitive pressure sensor based on a porous pyramid dielectric layer (PPDL) which, when compared to the conventional pyramid dielectric layer, had a significantly increased sensitivity of 44.5 kPa−1 in the pressure range <100 Pa. The high sensitivity was achieved by an increased deformation level of the porous dielectric materials, along with the pyramid architecture, which induces the highest pressure at the apex of the pyramids, where the cross-sectional area is the smallest [145] as shown in Fig. 2.7.

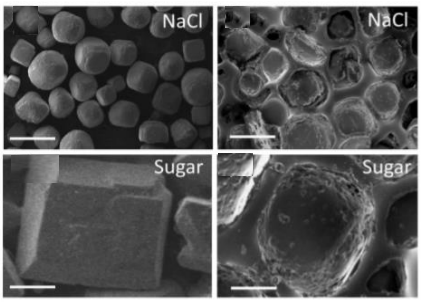

Source: L. Dana, S. Shia, H. J. Chunga, and A. Elias, "Porous polydimethylsiloxane–silver nanowire devices for wearable pressure sensors," ACS Appl. Nano Mater. 2019, 2, 4869−4878.

(a)

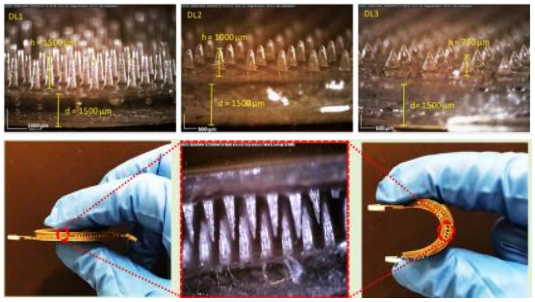

Source: V. Palaniappan et al., "Laser-assisted fabrication of a highly sensitive and flexible micro pyramid-structured pressure sensor for E-Skin applications." IEEE Sens. J., 2020, 20, 7605-7613.

(b)

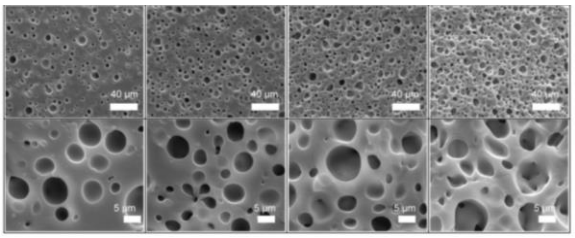

Source: S. Jang and J. Hoon Oh, "Rapid fabrication of microporous BaTiO3/PDMS nanocomposites for triboelectric nanogenerators through one-step microwave irradiation," Scientific REPORTS, vol. 2018, p.14287, 2018.

(c)

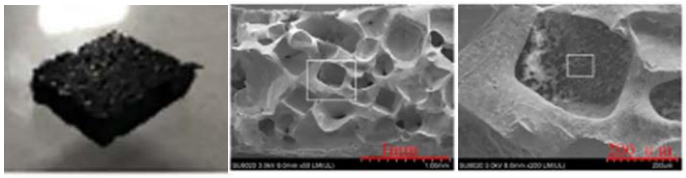

Source: P. Wei, X. Guo, X. Qiu and D. Yu, "Flexible capacitive pressure sensor with sensitivity and linear measuring range enhanced based on porous composite of carbon conductive paste and polydimethylsiloxane," Nanotechnology, vol. 30, p.455501,2019.

(d)

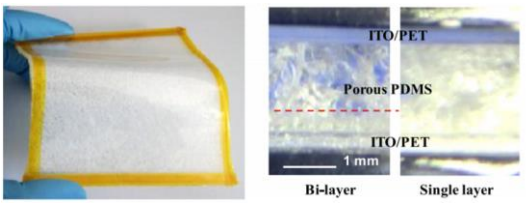

Source: S. Peng, S. Chen, Y. Haung, S. Pei, X. Guo, "High sensitivity capacitive pressure sensor with bi-layer porous structure elastomeric dielectric formed by a facile solution based process," IEEE Sensors Letters, vol. 3 (2), p. 2500104, Feb. 2019.

(e)

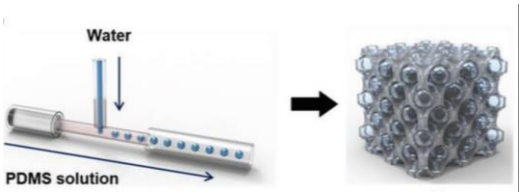

Source: J. Oh et al., "Highly uniform and low hysteresis piezoresistive pressure sensors based on chemical grafting of Polypyrrole on elastomer template with uniform pore size," Small, 2019, 15, 1901744.

(f)

Figure 2.6. Micro-structured pressure dielectric layers using different fabrication techniques: (a), sugar and salt 3D templates [143] (b) laser patterning [4] (c) drying water in PDMS [146] (d) carbon black filler in PDMS [147] (e) developing CO_2 gas in PDMS [148] and (f) injecting water droplets in PDMS [149].

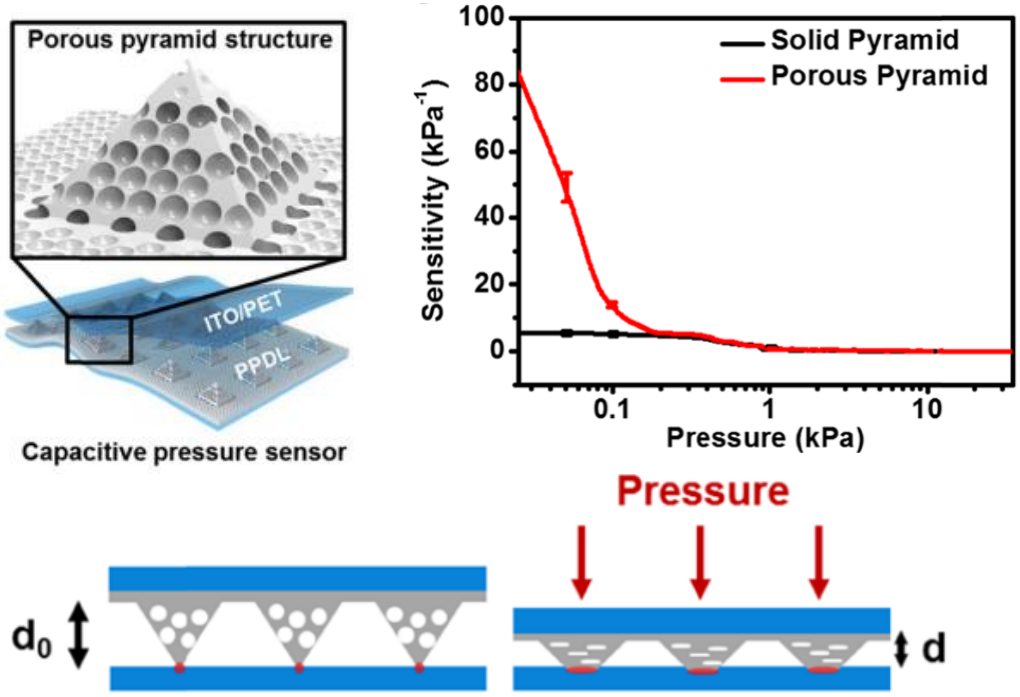

Figure 2. 7: Ultra-high sensitive capacitive porous pyramid structured pressure sensors consist of a dielectric layer sandwiched between two conductive electrodes [144]. *[Source: J. C. Yang et al, "Microstructured porous pyramid-based ultrahigh sensitive pressure sensor insensitive to strain and temperature," ACS Appl. Mater. Interfaces, 11, 21, 19472–19480, 2019]*

2.4. Sensor Data Acquisition and Processing Importance

Nowadays, due to the recent developments in the internet of things (IoT), a patient can be continuously monitored using wearable and off-body sensor-based devices at home [15,16]. In health monitoring systems, data acquisition is a significant stage in which the data acquired from sensors should be reliable to assess the health condition.

Data acquisition depends on the sensor as well as the environment in which the body signals will be recognized. After receiving the electrical signal by each sensor, data can be collected and converted to a readable digital format using a module embedded in the mobile device. However, the accuracy of the measured data can be affected by a variety of noises such as, weak contact between the electrode and the skin, electromagnetic interference caused by power line, baseline

drift caused by respiration, electrosurgical instruments, and patient's body movements. In order to transform these data to a meaningful and readable information, in addition to hardware, powerful software is also needed to reduce some of these noises and do possible processing and analysis [17,18].

Depending upon the environmental conditions, the types of sensor, the capabilities of the electronic readout module, types of the applications and the types of data collected, data processing methods can be defined or changed. Figure 2.8 shows the typical processing steps required after collecting the data [18]. Data processing methods may include a segmentation method, which divides a larger data stream into smaller chunks appropriate for processing, and a definition of the window size [18]. Healthcare services in terms of diagnostics and predicting modelling can also be improved by machine learning and artificial intelligence techniques [17].

Machine learning is a branch of artificial intelligence that can find arbitrary patterns or structure in data and make predictions for new input data [17]. To overcome the challenges associated with biosensors such as sensor drift and to make them as intelligent biosensors to

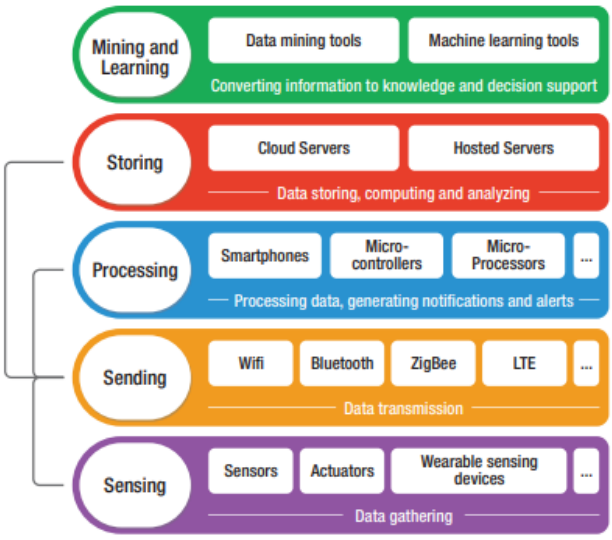

Figure 2.8. Post processing steps of the collected data from sensors [18]. *[Source: H. H. Nguyen, F. Mirza, M. A. Naeem and M. Nguyen, "A review on iot healthcare monitoring applications and a vision for transforming sensor data into real-time clinical feedback," Proceedings of the 2017 IEEE 21st International Conference on Computer Supported Cooperative Work in Design (CSCWD), 2017]*.

predict species based on decision system, machine learning can provide novel strategies. Recently, machine learning techniques such as regression, genetic algorithm, clustering, bayesian classification, fuzzy logic, neural network, κ-nearest neighbor (κNN), support vector machine (SVM), Naive Bayes (NB), decision tree (DT), gradient-boosted trees (GBT), random forest (RF), Feedforward artificial neural network (Feedforward ANN), recurrent neural network (RNN), and convolutional neural network (CNN) have been used for feature extraction and building decision models for prediction. Some of these techniques are commonly used in biosensors, while the others remained untouched by the biosensor community [14].

2.5. Summary

In this chapter, the author has provided a literature review on different types of sensors and sensing mechanisms. This was done by reviewing the FHE features and requirements, introducing different types of sensing mechanisms and introducing different types of pressure sensing transducers. The author introduced some of the wearable pressure sensors used for remote health monitoring by highlighting the cone-structured porous capacitive pressure sensing. The importance of the sensor data acquisition system in any sensing and monitoring device was also reviewed.

CHAPTER III

HIGHLY SENSITIVE CONE-STRUCTURED POROUS PRESSURE SENSORS FOR RESPIRATION MONITORING APPLICATIONS

3.1. Introduction

Wearable devices and health monitoring apps have recently gained a lot of momentum and are altering the way patients' access/receive healthcare services. Wearable technology refers to a category of electronic devices that can be worn as accessories, embedded in clothing, implanted in the patient's body, or even tattooed on the skin [1-13]. These wearable devices are peel and stick patches and can be used for continuous monitoring of diverse human physiological activities such as cardiac pulse and gait analysis. Coronavirus (COVID-19) has spread globally since late 2019 and has affected the day-to-day life of millions of people worldwide. Throughout this pandemic, the extreme demand for the clinical equipment such as intensive care unit (ICU) resources have resulted in a disruption of medical supply chain, even in developed countries. In the USA, almost 14 million confirmed cases and more than 260,000 deaths has been reported as of December 1, 2020 [19]. As per the data from 555 US medical centers, a total of 192,550 adults hospitalized with COVID-19, and among them 55,593 (28.9%) were admitted to ICU. Severe hypoxic respiratory failure requiring mechanical ventilation is the most common reason COVID-19 patients are admitted to the ICU.

Respiration monitoring has been a critical parameter in estimating the lung volume and perfusion, and in turn monitoring the severity of the disease for patients with COVID either in the ICU or regular wards or at-home treatment. Typically, hospitals are equipped with advanced oximetry equipment to monitor the respiration rate. However, recently, due to the COVID-19 pandemic, there has been a huge disparity between the availability of these devices and the

number of patients who need it [20-23]. To cover this disparity/gap, there is a need to develop and employ more accessible devices using novel wearable technology capable of monitoring the respiration rate.

Flexible pressure sensors have been developed for object detection, structural monitoring and gait analysis in various applications. Recently, the development of highly sensitive pressure sensors for monitoring respiration has gained attention and are envisioned for applications in continuous respiration rate monitoring and early detection of the patient's respiration failures [24,25]. Pressure sensors should be highly responsive (sensitive) and detect pressures in range of 0-2 kPa in order to detect different respiration rates [26]. Among the different types of pressure sensors, capacitive based pressure sensors are reported to be highly responsive which can be achieved by varying the design parameters and properties of dielectric layer [151,161]. The sensitivity of the pressure sensors has been enhanced by creating micro-structured dielectric layers (such as polydimethylsiloxane (PDMS)) using various prototyping techniques including 3D sacrificial templates such as sugar, micropatterning such as micro pyramid/cone, and developing chemical reactions for creating gas pockets [10, 162-164]. Among these techniques, gas pockets and cone structures resulted in high sensitivity. However, there is no research available on the development of pressure sensors with dielectric layers made of hybrid microstructures (combined two or more microstructures). It is envisioned that pressure sensors developed with hybrid micro-structured dielectric layers will result in ultra-high sensitivity sensor for respiration rate monitoring applications [143,6,165].

In this project, a highly sensitive capacitive pressure sensor, with dielectric layer made of pores and cone structures, was fabricated and its capability to detect varying low pressures was investigated.

3.2. Experimental

3.2.1. Chemicals and Materials

Sylgard® 184 silicone elastomer kit (A & B) from Dow Corning; $NaHCO_3$ powder; HNO_3 (70%) and 99.5 % anhydrous isopropyl alcohol (IPA) from Sigma-Aldrich chemical company; were used for the fabrication of porous dielectric layer. A stretchable sweat resistant polyester and polyurethane based fabric (JenniferS/914) from Top Value Fabrics Inc; silver (Ag) ink (Ag800) from Applied Ink Solutions; a stretchable thermoplastic polyurethane (TPU) material (Intexar TE-11C) from Dupont, were used for fabricating the top and bottom electrodes. Formlabs high temp resin (RS-F2-HTAM-02) was used for the fabrication of the 3D printed mold.

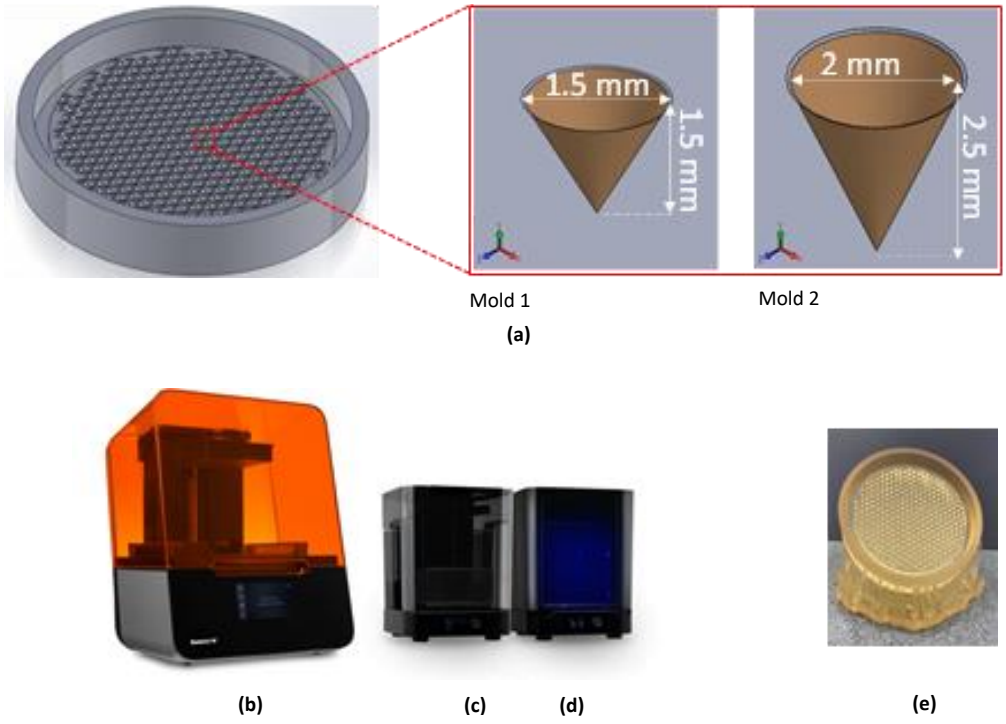

Figure 3.1. Master mold fabrication process: (a) CAD design for two molds with different cone dimensions, (b) Form 3 Formlabs 3D printer, (c) Form wash (d) Form cure and (e) 3D printed master mold.

3.2.2. Fabrication of the 3D Printed Master Molds

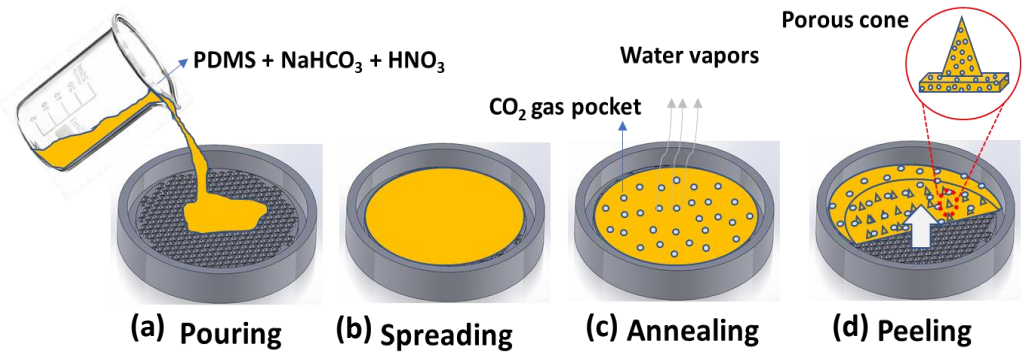

Figure 3.2. Dielectric layer fabrication process: (a) pouring the mixture of PDMS, $NaHCO_3$, and HNO_3 into the 3D printed mold, (b) waiting until proper spreading of the mixture (c) annealing and (d) peeling the porous cone structured layer.

Master molds for the fabrication of the porous cone structured PDMS dielectric layer were prepared using a rapid and precise 3D printing technique. Initially, a mold with inverted cone grooves was designed in SolidWorks software. As illustrated in Fig. 3.1(a), two master molds with cones of different height and base width were designed. As shown, mold-1 and mold-2 were designed with inverted cone grooves of 1.5 mm × 1.5 mm, and 2 mm × 2.5 mm, respectively (the pitch was 2.25 mm for both molds). Then, the CAD file was imported into a Form 3 3D printer machine (Fig. 3.1(b)) and the master mold was printed at a resolution of 50 microns by melting the high temperature clear resin. Table 3.1 shows some of the 3D printing properties. The printed mold was then transferred to the Form-wash (Fig. 3.1(c)) and washed with isopropyl alcohol (IPA 91%) for six minutes. Following this, the printed mold was cured in the Form-cure (Fig. 3.1(d)) for 120 minutes at 80 °C. The photograph of the 3D printed master mold (mold-1) is shown in Fig. 3.1(e).

Table 3.1. 3D printing properties.

Technology	Resin Fill System	Layer Thickness (Axis Resolution)	Laser Spot	XY Resolution
Low Force Stereolithography (LFS)™	Automated	50 – 300 µm	85µm	50µm

3.2.3. Fabrication of Porous Cone Structured Pressure Sensor

Sylgard® 184, composed of a 10:1 ratio of elastomer base to curing agent (w/w)) was mixed with 20% (w/w) $NaHCO_3$. HNO_3 was added to the PDMS−NaHCO3 mixture (20% compared to PDMS (w/w)), followed by manual stirring for 5 minutes. Following this, the mixture was poured into the molds and left for 60 minutes to obtain a proper spread and fill of the PDMS mixture into the grooves (Fig. 3.2(a,b)). After that, the mold was placed in a drying oven (Yamato DX300) and the mixture was thermally annealed for 30 minutes, at 130 °C (Fig. 3.2(c)). During annealing process, an acid−base neutralization process occurs resulting in the creation of CO_2 gas pockets

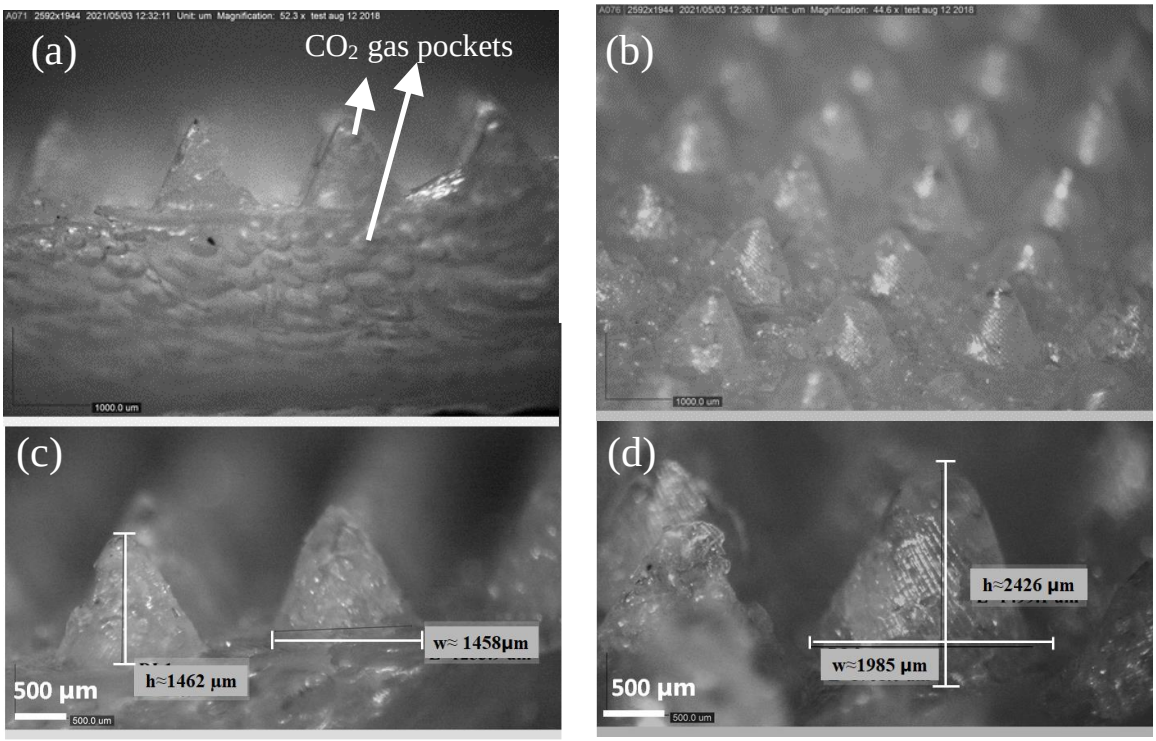

Figure 3.3. Microscopic images of the fabricated porous cone structured dielectric layers:.(a) side view (b) top view, and (c,d) close view of the cones fabricated using mold 1 and mold 2.

in the PDMS mixture along with water vapors and sodium nitrate ($NaNO_3$) as byproduct [6,148]. Finally, the PDMS dielectric layer, with pores and cone structures, was peeled off from the mold (Fig. 3.2(d)). Then, the dielectric layer was immersed in a diluted solution of IPA and sonicated in deionized (DI) water for 30 minutes for removing the byproduct $NaNO_3$. The microscopic images (captured using a Dino-Lite digital microscope) of the dielectric layers with different cone dimensions are shown in Fig. 3.3. As shown in Fig. 3.3(a), CO_2 gas pockets (porous structures) were formed both in the cones and the base layer regions of the dielectric layer. Figure 3.3(b) depicts the uniform formation of the cones on the surface of the porous PDMS layer. As illustrated in Fig. 3.3(c,d), height and width of the porous cone structures were measured to be ≈1462 mm, ≈1458 mm (mold-1); and ≈2426 mm, ≈1985 mm (mold-2), respectively. Then, the top and bottom electrodes were fabricated by screen printing Ag square blocks on a TPU substrate that was heat-laminated onto a fabric. Finally, the dielectric layer and electrodes were laser cut (PLS6MW 10.6 μm CO_2 laser beam from Universal Laser Systems) into circles with a diameter of 35 mm and the pressure sensor was assembled by sandwiching the dielectric layer between the electrodes [145]. The photograph of the fabricated pressure sensor with cone structured porous dielectric layer and fabric electrodes is shown in Fig. 3.4.

The fabricated pressure sensors were characterized by placing the sensor between a force gauge (M5-5) and a compression plate, in a motorized test stand (Mark-10 ESM 301). The force gauge was used to apply varying pressures (0 kPa (no load) to 10 kPa). The pressure sensor was connected to an LCR meter (Agilent E4980A) for measuring the capacitive responses for varying applied pressures. A software was developed with a custom-built Visual Studio C# program to control the force gauge and sensor data acquisition.

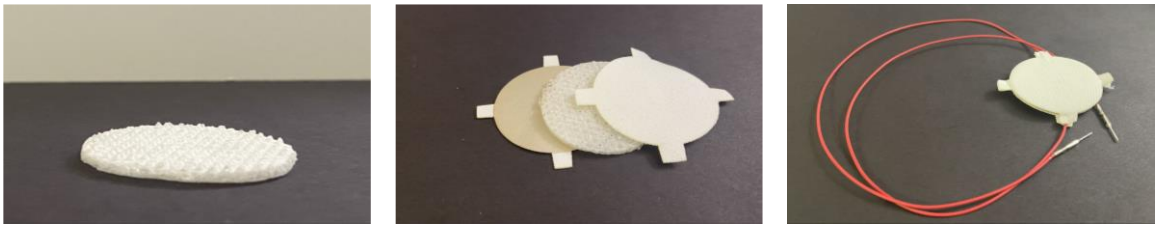

(a) (b) (c)

Figure 3.4. Photographs of the pressure sensor: (a) cone structured porous dielectric layer, (b) sensor layers including dielectric layer between fabric electrodes and (c) fabricated cone structured porous pressure sensor.

3.2.4. Results and Discussion

Capacitive responses of the fabricated pressure sensors were investigated for three applied pressure ranges of 0 to 100 Pa in steps of 5 Pa, 100 Pa to 2 kPa in steps of 0.1 kPa, and 2 kPa to 10 kPa in steps of 2 kPa, with a dwell time of 5 seconds. To investigate the effect of the pores (created by the CO_2 gas pockets) as well as the cone structures (formed by the 3D printed master molds) of the PDMS dielectric layer on the sensitivity of the pressure sensor, four types of sensors were tested, and the results were compared. These pressure sensors include porous cone-1 (1.5×1.5 mm), porous cone-2 (2×2.5 mm), non-porous (solid) cone (2×2.5 mm), and porous no-cones (even surface).

Figure 3.5(a) shows the dynamic response of the sensors for an applied low pressure of 5 Pa. The porous cone-1 and 2 clearly shows a higher capacitance change when compared to the non-porous cone and porous no-cones pressure sensors. The capacitance change of the porous cone-2 is significantly high (by 30%) when compared to porous cone-1. An overall relative capacitance change of ≈ 114, ≈ 108, , ≈ 83, ≈ 32 was obtained for porous cone-2, porous cone-1, non-porous cone, and porous no-cones when the pressure was varied from 0 to 10 kPa, respectively (Fig. 3.5(b)). The porous cone-2 showed the highest sensitivity of ≈135 $\%kPa^{-1}$, ≈25 $\%kPa^{-1}$, and ≈5 $\%kPa^{-1}$ for all the applied pressure ranges (0 to 100 Pa, 100 Pa to 2 kPa, and 2 kPa to 10 kPa). The hysteresis response of the porous cone-2 was investigated by applying stepwise continuously increasing pressures from 0 kPa up to 10 kPa followed by continuously decreasing pressures to 0 kPa (steps of 1 kPa), as shown in Fig. 3.5(c). An average degree of hysteresis of 4.3% was then calculated for the porous cone-2. In addition, repeatability of porous cone-2 was investigated by subjecting it to 200 cycles of three pressure loadings of 100 Pa, 2 kPa and 10 kPa. As shown in Fig. 3.5(d), porous cone-2 demonstrated a highly stable capacitive response with a relative capacitance change of 2.9%, 3.1% and 3.9% when compared to the base value, for the applied pressures of 100 Pa and 2 kPa, and 10 kPa, respectively.

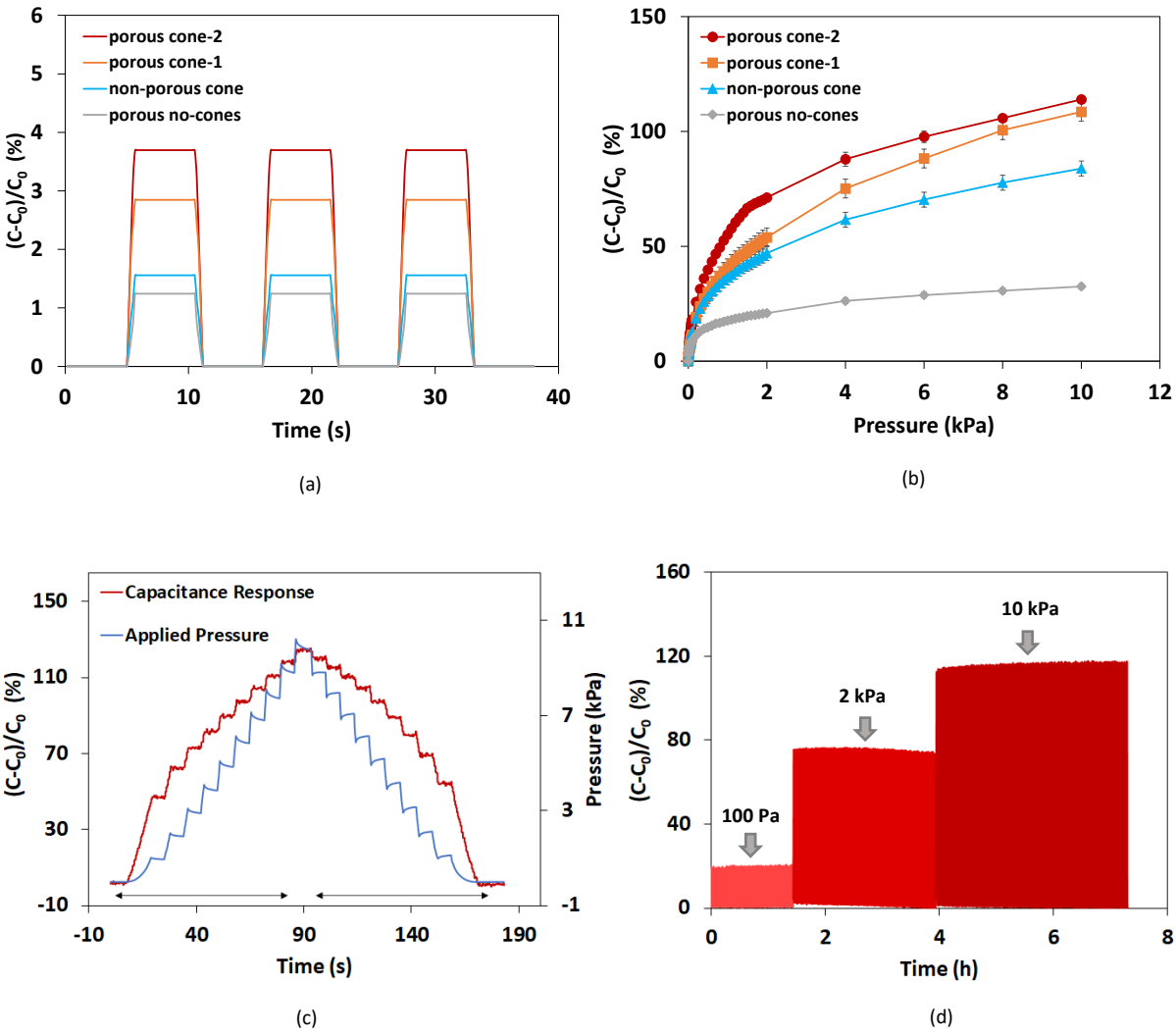

Figure 3.5. Capacitive response of the fabricated pressure sensors: (a) dynamic response for the applied very low pressure of 5 Pa (b) relative capacitance change response (c) step wise pressure response and (d) repeatable capacitive response of the porous cone-2 under the application of multiple cyclic pressures.

In addition, the capability of the pressure sensor (porous cone-2), with the highest sensitivity, to detect very low-pressure ranges was demonstrated by measuring the pressure applied onto a mask by the air flow while breathing. Some of the general human respiration characteristics are included in Table 3.2. Normal breathing includes inhalation, exhalation which takes roughly 3 to 4 seconds, followed by a short pause of 1 to 2 seconds with no breathing as shown in Fig. 3.6.

Table 3.2. Human respiration characteristics.

Respiration characteristics	**Normal rates**
Inhalation	1.5-2 s
Exhalation	1.5-2 s
Automatic pause	No breathing for 1-2 seconds
Minute ventilation (MV)	6 L/m (for a 70 kg man at rest)
Tidal volume (TV)	500 ml - air volume breathed in during a single breath
Respiratory frequency (Rf)	12 breaths per min (can be up to 20)

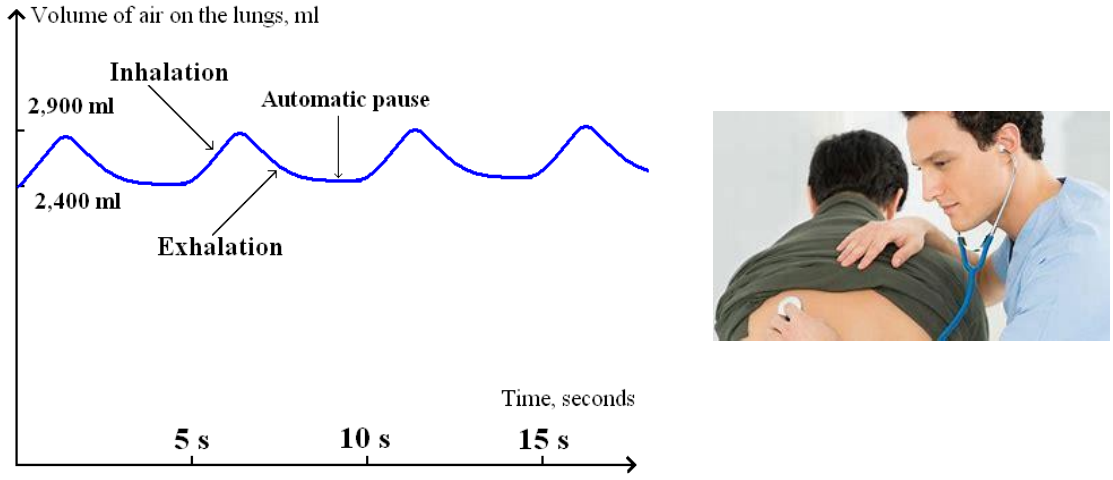

Figure 3.6. Normal breathing pattern of human in time. *[Source: https://www.normalbreathing.com/respiratory-rate-volume-chart/]*

For a healthy adult, a normal respiration rate is usually between 12 to 20 respiration per minute with a minute ventilation of 6 L/min [165]. A fabric based porous cone pressure sensor was sewed inside a surgical mask and the mask was worn by a male subject. It was observed that sensor was capable of detecting different respiration rates. As shown in Fig. 3.7(a), normal, fast, and deep breathing cycles were clearly detectable from the capacitance change. An average capacitance change of ≈ 3% was recorded when the subject was breathing normally and then the capacitance change increased to ≈ 5% and ≈ 10% by increasing the respiration rate to the fast and deep states,

respectively (Fig. 3.7(a)). This clearly shows that the sensor is capable of detecting different respiration rates and can be potentially employed for continuous monitoring of respiration.

In addition, an air flow controller system and an isolated air-tight chamber box was set up for measuring the capacitive responses of the sensor for different rates of the air flow (Fig. 3.7(b)). A software was developed in Visual studio C# program for controlling the air flow channels, data acquisition and analysis (Fig. 3.7(c)). The pressure sensor was placed inside the chamber box and a relative capacitance change of ≈0.3%, ≈0.5% and ≈1% was obtained when the air flow was set

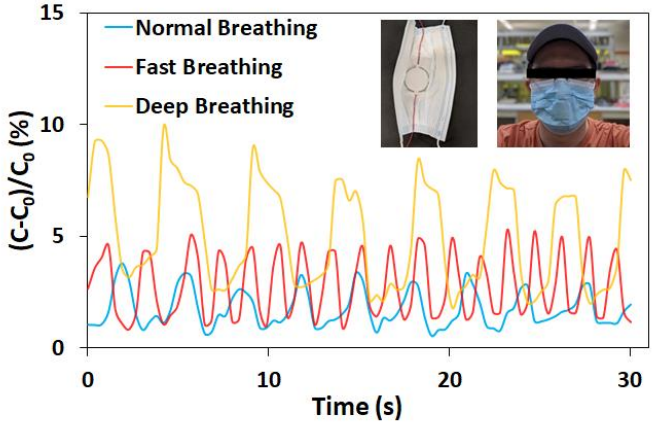

(a)

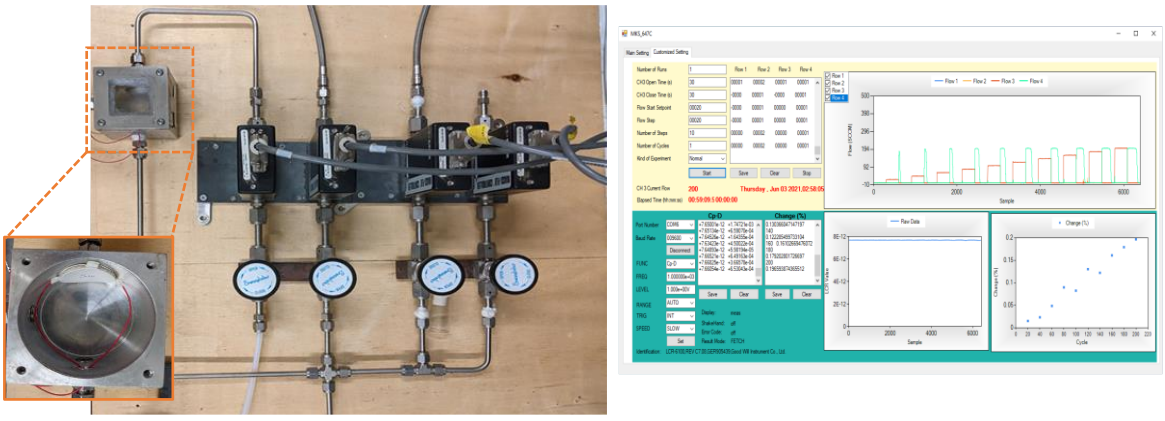

(b) (c)

Figure 3.7. Respiration and air flow rate monitoring: (a) respiration rate detction using cone structured porous pressure sensor attched to the mask, (b) air flow controller system with an isolated air-tight chamber (inset - lid off) for placing the pressure sensor and (c) developed software.

to ≈ 0.15 L/min, ≈ 0.2 L/min and ≈0.3 L/min (≈40 times less than the flow of the real breathings – considering that the regular breath flow is ≈6 L/m). These results demonstrated that the cone structured porous pressure sensor is highly sensitive to air flow even for the flow ranges less than the breath flow. Currently, more research work has been focused on establishing a correlation among the respiration rate of human and the adjusted airflow in the chamber, by performing the capacitance measurements of the sensor.

3.2.5. Summary

The outbreak of the COVID-19 crisis has significantly expanded the role of wearable technologies for the continuous monitoring of various health metrics to address real-life problems. In this direction, a novel highly sensitive fabric based flexible pressure sensor was fabricated using 3D printing processes and additive screen printing. A high sensitivity of ≈530% kPa^{-1} was measured for the sensor for ultra-low-pressure ranges below 10 Pa. The pores and cone structures provided excellent deformation and clearly showed higher sensitivity when compared to the plain non-porous/non-cone sensors. A fabric-based sensor was sewed inside a surgical mask and the sensor was capable of detecting different human respiration rates.

CHAPTER Ⅳ

DEVELOPMENT OF SOFTWARE FOR FORCE TEST STAND MODEL ESM301 AND MULTI-CHANNEL FLOW RATIO/PRESSURE CONTROLLER TYPE 647C FOR MACHINE LEARNING PURPOSES

4.1. Introduction

In any sensing and monitoring device, the data acquisition system (DAQ) plays an important role as it collects data from different sensors. This data should be digitalized for storage and sent to a control center for performing the processing and visualization. A basic DAQ system contains four key components including; sensor interface, signal conditioning, analog to digital conversion, processing and transmission of the data. Typically, sensors can be identified as the first stage of the monitoring system to convert a physical quantity into an electrical signal that can be measured and read by an electronic system. In order to collect valid and reliable data from sensors and reducing the measurement errors, it is crucial to eliminate any external effects such as human interference when recording the data. Moreover, for providing long-term reliable data, the sensor lifetime can be determined by examining it under the application of continuous and uniform amounts of the appropriate physical stimuli in an accelerated way.

To eliminate the human interferences as well as predicting the sensors performances in long term use cases, the author was motivated to develop automated pressure sensing and flow measurement systems. The automation was made possible by developing software to control the movement of a force gauge as well as a flow controller device. In this chapter, the development of the software, related flowcharts, and the process flow of the main functions are discussed. The C# codes and PC control commands for both software are available in the Appendix.

4.2. Software Development for Controlling the Force Test Stand

In order to perform experiments on the fabricated capacitive pressure sensors properly, a controllable, repeatable and robust experiment setup is required. The measured capacitance change and the calculated sensitivity values will not be valid if the pressure has not been applied uniformly from experiment to experiment. The measurement errors originated from the human interference has remained unavoidable even when well trained technicians are employed. Therefore, rather than relying on humans, employing a software-based controller to provide the desired applied force (which in turn provides the required displacement on the force stand machine) is preferred. At the same time, when the force is being applied to the sensor, we need to record the electrical signals (capacitance) that are varying as the result of a change in the sensor structure. In this work, varying pressures were applied to the pressure sensors using different force gauges, M5-5 (0-20 kPa), M5-50 (20- 200 kPa), and M5-200 (200-1000 kPa). The sensors were mounted between the force gauge and a compression plate of a motorized test stand (Mark-10 ESM 301). An LCR meter (Instek LCR-6100) has been used for recording the capacitance

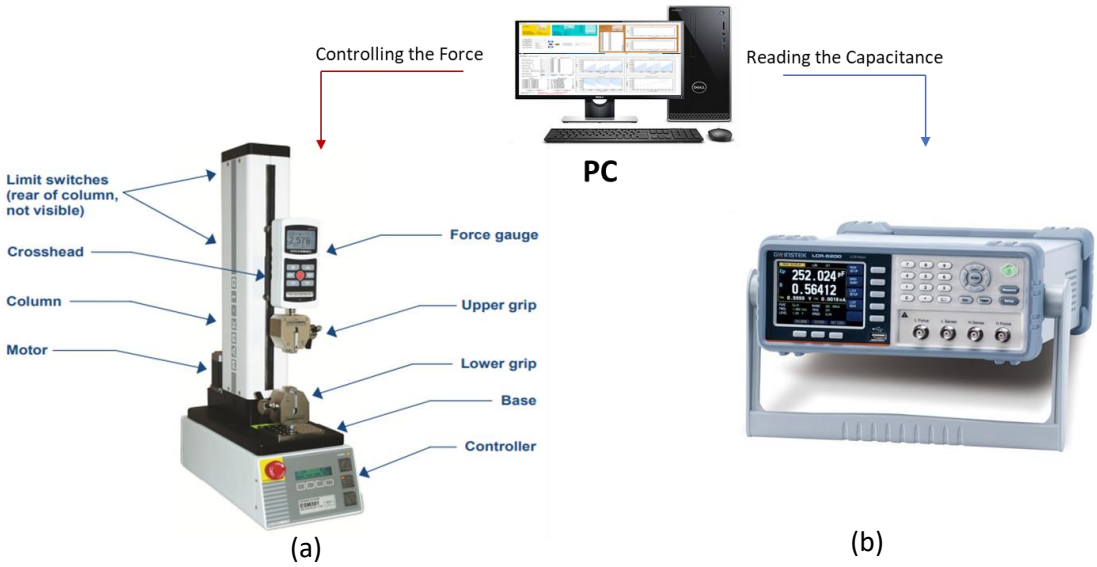

Figure 4.1. (a) Force test stand model ESM301 and (b) LCR meter (Instek LCR-6100).

response of the pressure sensors. Figure 4.1 shows the Mark- 10 ESM 301 test stand and the Instek LCR-6100.

The developed software has the capability to compute the relative percentage changes of any measured parameter (inductance, capacitance, and resistance) and plot the obtained results on a computer. The LCR meter can be disconnected only if the applied force and displacement are to be calibrated. This will also increase the speed and the accuracy of the software for detecting the force set points. Figure 4.2 shows the flow charts of the main function and critical routines of the developed software. The main functions includes:

- Finding the available COM ports for communicating with the machine
- Connecting to the force gauge machine
- Reading the settings on LCR meter and force gauge machine
- Initiating the test.

When the “Main Form” of Visual Studio C# is executed, available COM ports will be recognized (found), and then the main and customized setting tabs will be displayed. Next, the software can be connected to the machine by selecting the corresponding COM port and using the “Connect” option on the software. After that, all available settings will be read and shown on related textboxes and labels. In read/write setting function, when the LCR meter is not available, the software will skip performing the read/write function for LCR meter.

The software contains two major tabs including “Main Settings” and “Customized Settings”. Figure 4.3 shows the “Main Settings” tab and this facilitates adjusting the connections to the force gauge machine and LCR meter in the yellow and green panels, respectively. In addition, the force gauge settings can be adjusted according to the experiment. For example, the travel units (in or mm), crosshead (for activating the speed setting tab), operation mode (cycle, limit, manual), speed, and upper/lower travel limits (mm) can be adjusted using the buttons in the relevant textboxes. This “Main Settings” tab is very crucial to automate the machine for testing. For example, when performing experiments on pressure sensor, the set point must be detected by the up and down buttons (on the force stand) where the force gauge touches the pressure sensor at a minimum pressure. After detecting the set point, the vertical displacement of the force gauge on the force stand can be reset to zero by pressing the reset button. In addition, the force gauge can also be reset to zero force. Force and displacement adjustments can be monitored using “Data

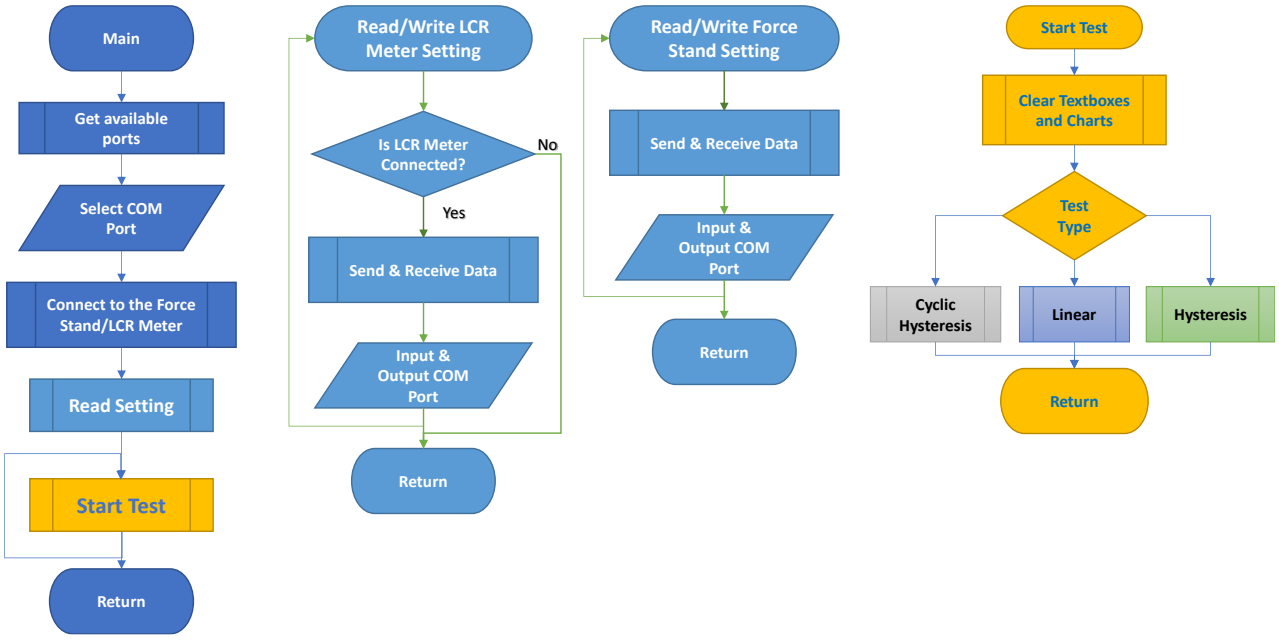

Figure 4.2. Main function and critical routine flowcharts.

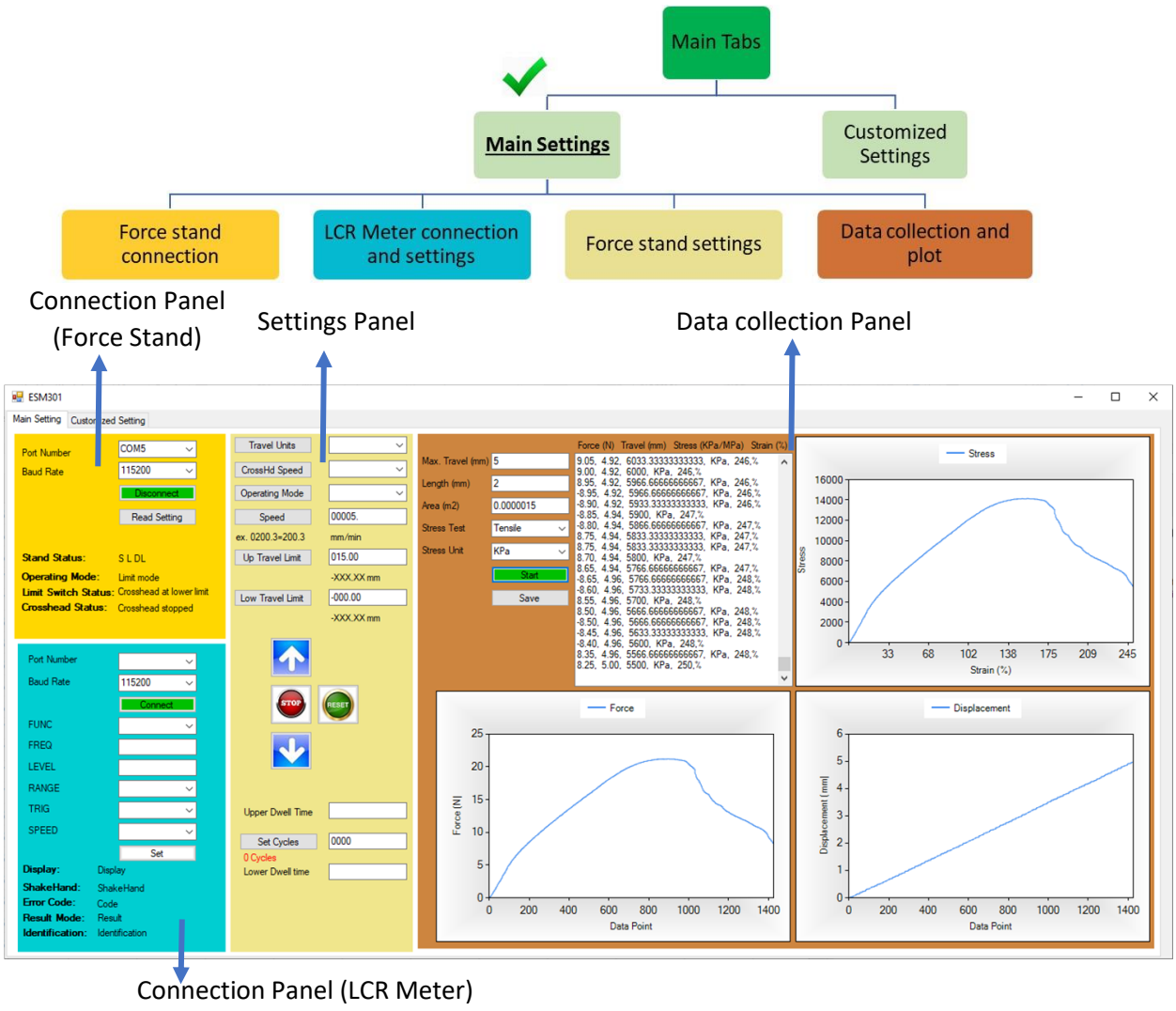

Figure 4.3. Main settings page.

Collection" panel.Once the "Main Settings" are completed for running the experiment, the "Customized Settings" (in the second tab) can be defined for three different types of test. The "Customized Settings" tab is shown in Fig. 4.4. Depending on the force gauge model and the kind of experiment selected from the yellow box, the number of runs, upper and lower dwell time, force start point, force steps, number of steps, number of cycles, upper and lower speed, and the resolution can be defined by the operator. When the displacement is not zero the software detects the displacement as a set point. Three differend types of experiment including linear, cyclic, and hysterysis can be defined and selected from the "Experiment Type" option, which are discussed

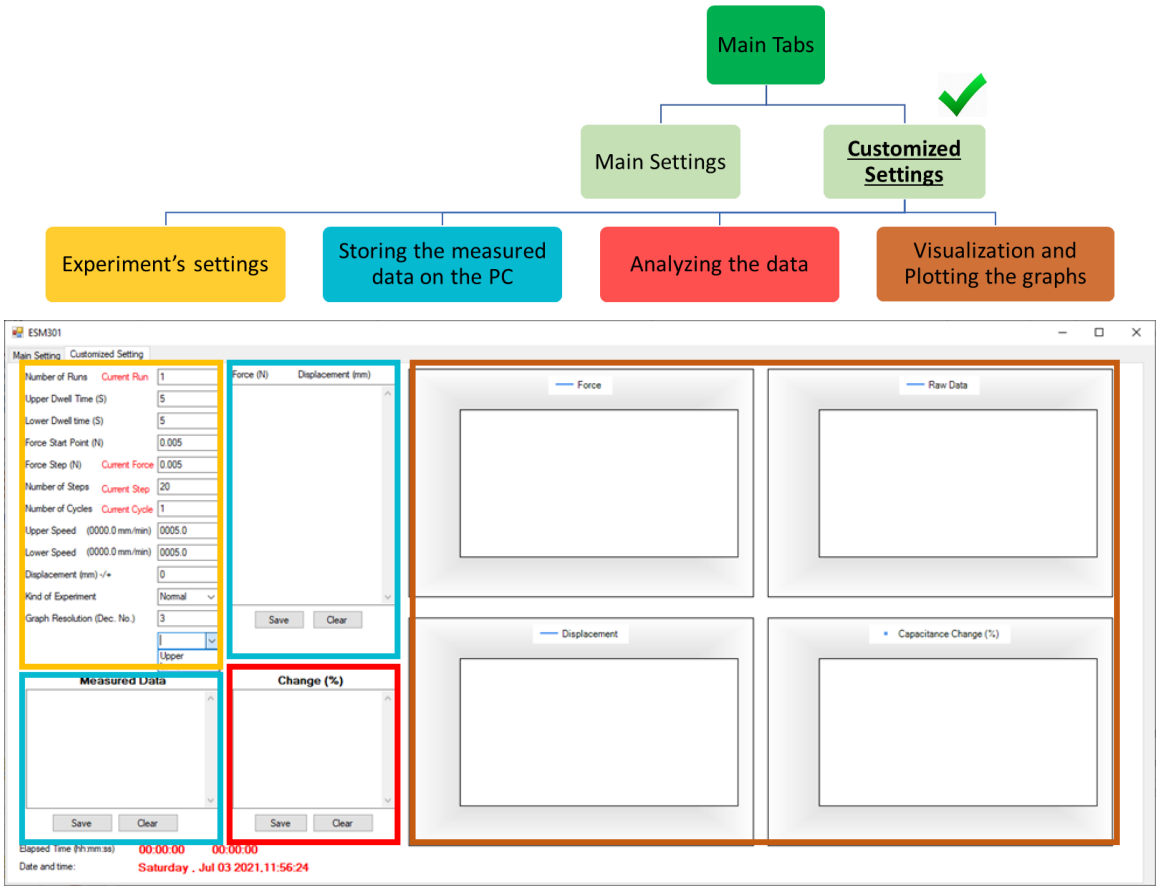

Figure 4.4. Customized settings page.

in the following sections. In "Customized Settings" tab, experiment settings for the force gauge machine can be adjusted in the gold box. The green boxes, in "Customized Settings" tab, show the measured raw data that will be collected from the force gauge and LCR meter. The red box displays the analyzed data. Force, displacement, capacitance, and capacitance change graphs will be provided in the brown box.

The developed software has four functions (Upper Limit, Lower Limit, Moving Up and Moving Down) for collecting data from LCR meter (sensor response) at different positions of force gauge. The four functions can be placed in a loop to move the force gauge continuously in a cyclic fashion. Procedures as well as the condition to break the loop is shown in orange flowcharts for different types of tests in Fig. 4.6, Fig. 4.8, and Fig. 4.10.

4.2.1. Linear Test

The linear test will be initiated after pressing the start button, when the setting and "Experiment Type" are selected as a linear test (Fig. 4.5). The timer and date (shown in red color in Fig. 4.5) included in "Customized Settings" tab helps to identify the exact sampling rate in each experiment. According to the flowchart shown in Fig. 4.6, after pressing the start button, a stopwatch based timing function will start, and the compiler runs the first cycle for the first force step point. In linear test, there are four main stages as shown in the flowchart of Fig. 4.6. For each cycle, in stage one, the force gauge value will be acquired when it is stopped by calling a function that can write commands to force stand and read its response. If LCR meter is connected, this function can return the average of capacitance which will be measured by LCR meter. During each communication between the Force Gauge and LCR meter through the developed software, the raw data from LCR meter, force and displacement values will be transmitted to the software

Figure 4.5. Linear test settings and results.

and the corresponding charts will be updated. The updating loop will break when the set time is

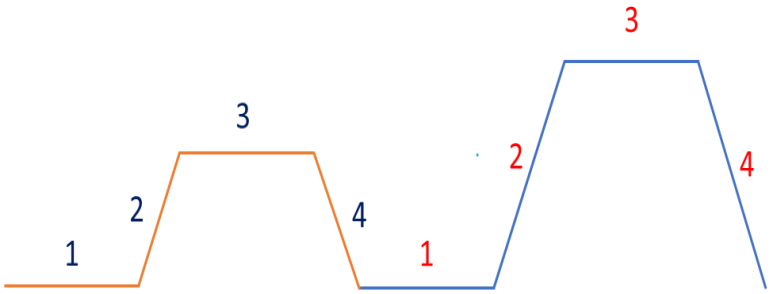

(a)

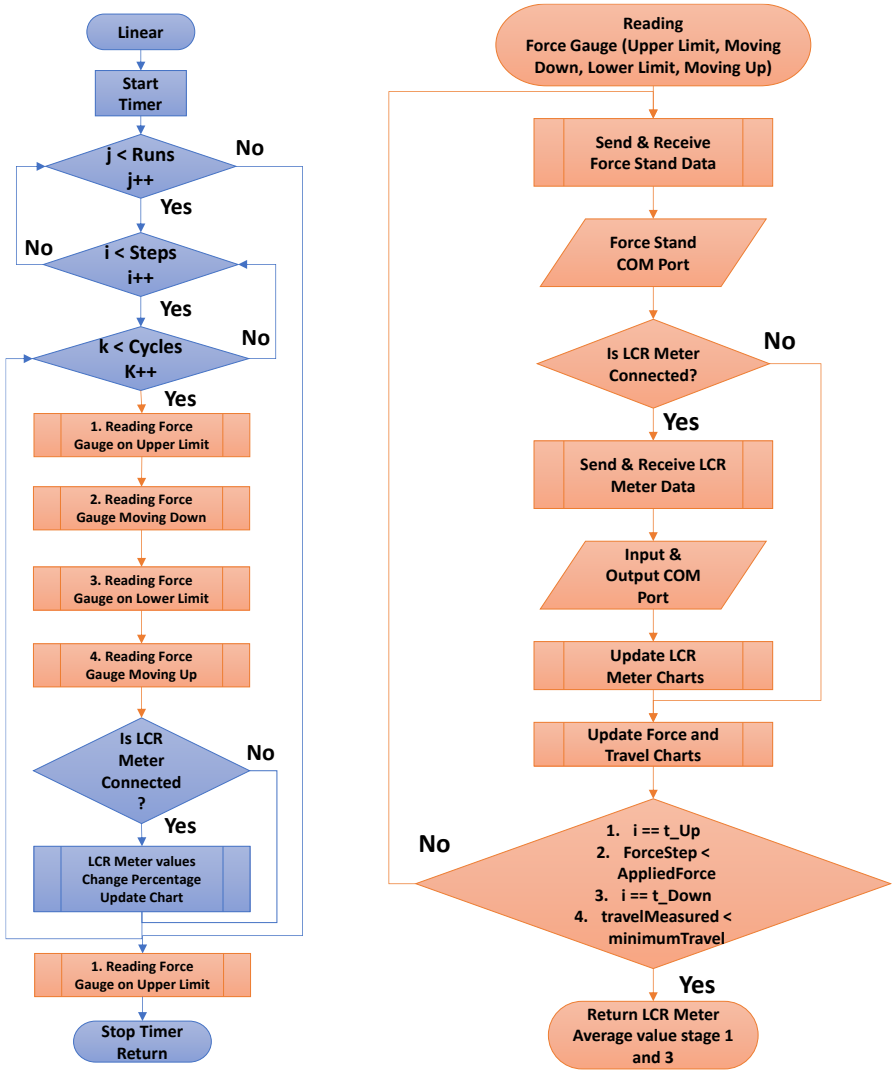

(b)

Figure 4.6. Linear test procedure, (a) stages, (b) flowchart.

over. Consequently, the Move Down command will be sent to the force stand during stage two. After command completion force, displacement and LCR meter values will be read again in this function. When the applied force value is larger than the force set point - the loop will encounter a break in this case and the force gauge stops at this point. In stage three, when the force gauge stops, it calls function to read and return force, displacement, and average LCR Meter values. The loop will encounter a break and end when the set time completes. In stage four, Move Up command will be sent to the force stand, then force gauge moves up and stop at zero displacement. During all of these four stages, charts will be updated in real time. When the compiler presets to the main linear function, capacitance change will be calculated based on two values from stage one and three. This process will be repeated in loop.

4.2.2. Cyclic Hysteresis Test

When the "Experiment Type" is selected as cyclic hysteresis as shown in Fig. 4.7, by pressing the start button, the cyclic hysteresis test will run. The timer and date will aid in determing the exact sampling rate employed/set for each experiment.

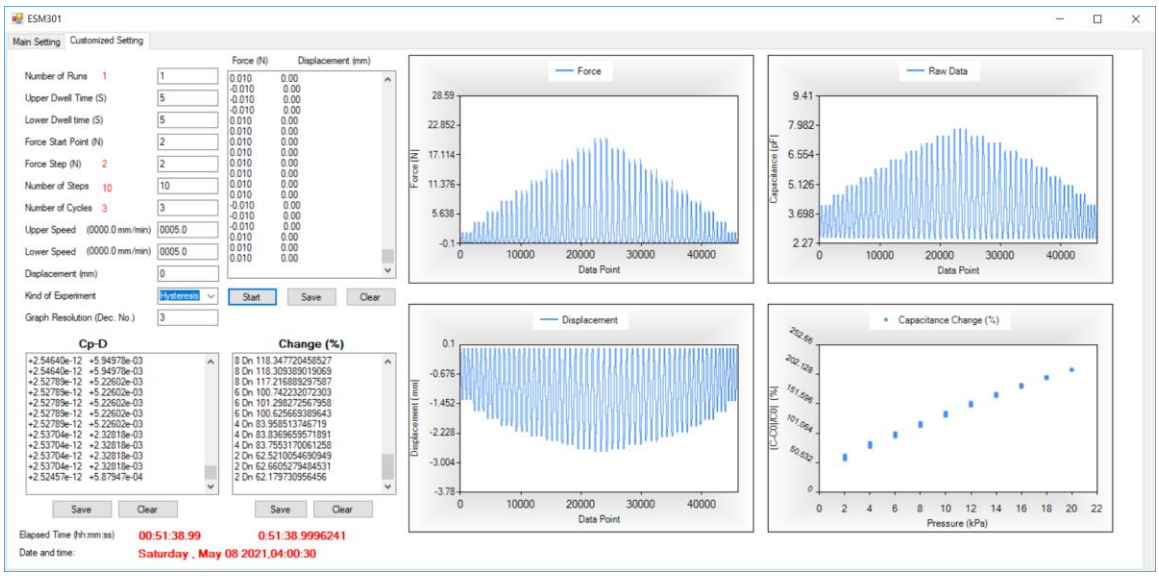

Figure 4.7. Cyclic hysteresis test settings and results.

Based on flowchart in Fig. 4.8, after pressing the start button, the stopwatch will start and the compiler runs the first cycle from the force step point. For each stage, a force gauge value is read when it is stopped, by calling a function that can write the commands to the force stand and acquire its response. If the LCR meter is connected, this function will also return the average of capacitance which is measured by LCR meter. The LCR meter raw data, force, and displacement charts will be updated in real-time continuously. The reading function loop in stage one will break when the set time is over. To continue the procedure of test in this cycle, the software sends the command to the force stand to move down. Force, displacement and LCR meter value are read again in this function, but if the applied force is larger than the force set point, the loop will encounter a break condition and the force gauge will stop at this point. When the force gauge is stopped in stage three, it calls the function three to read and return the average LCR meter value. In stage four, force gauge moves up and stops at zero displacement. During all these four stages, charts are being updated real time. Capacitance change will be calculated based on two values from stage one and three, when the compiler returns to the main function. This process will be repeated for each cycle in loop. Once the force step reach the last step in the cycle, it goes down sequentially in a step by step fashion.

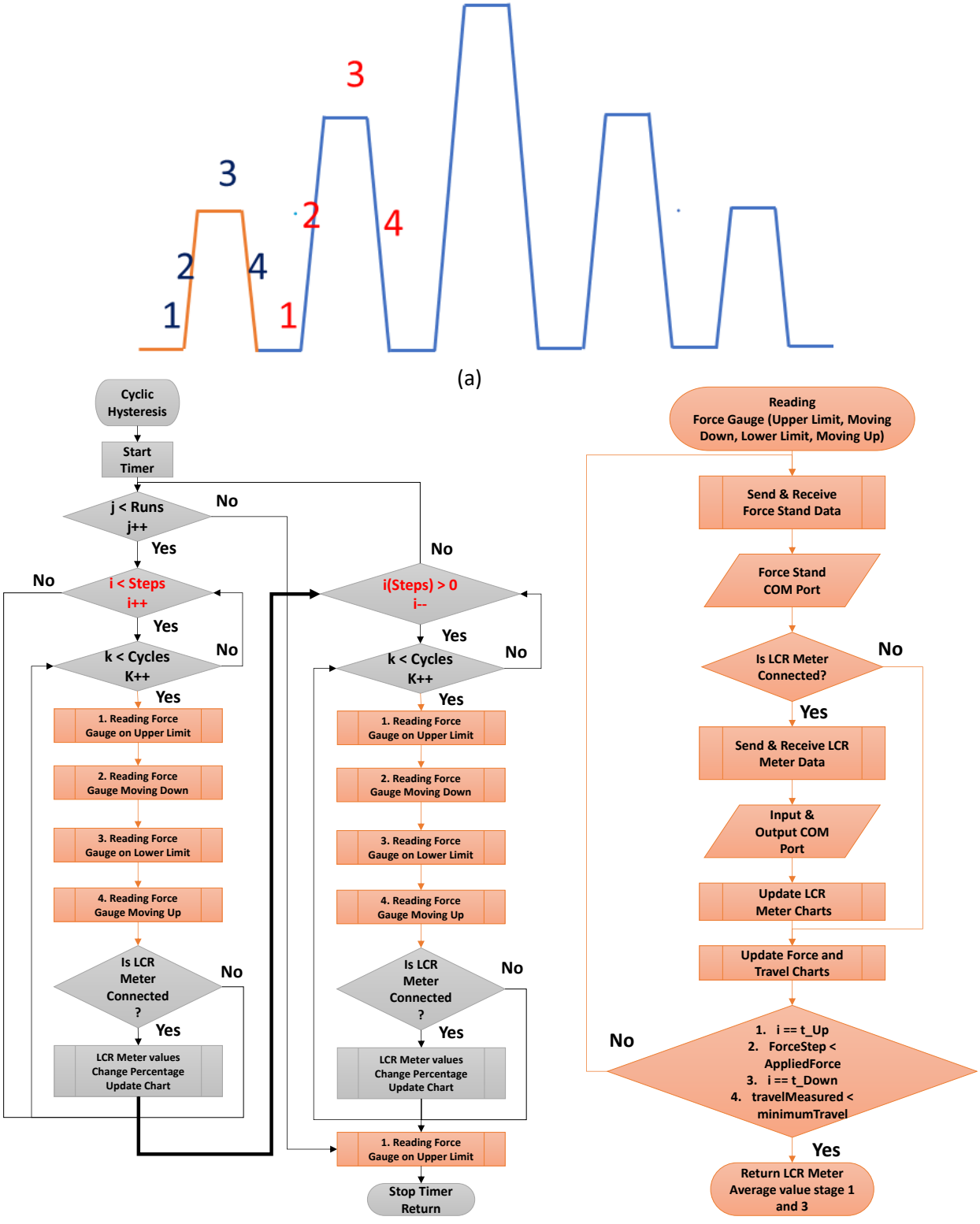

Figure 4.8. Cyclic hysteresis, (a) stages, (b) flowchart.

4.2.3. Hysteresis Test

The hysteresis test process will run after pressing the start button, when the “Experiment Type” is selected as hysteresis test (Fig 4.9). The timer (stopwatch) and date helps in providing the exact sampling rate for each experiment. According to the flowchart in Fig. 4.10, after pressing start button, the count-down in the stopwatch function will start, and the compiler will run the first cycle from the force step point. For each cycle, force gauge value will be read and record as a base average capacitance value when it is stopped by calling “Upper Limit” function on stage one. If LCR meter is connected, this function can return the average of capacitance which is measured by LCR meter. The LCR meter raw data, force, and displacement charts will be updated continuously. The loop will break when the set time is completed. In stage one, when the data is recorded for specific time, the average value will be returned, Next, by calling related function in stage two, the software sends the command to the force stand to move down. Force, displacement

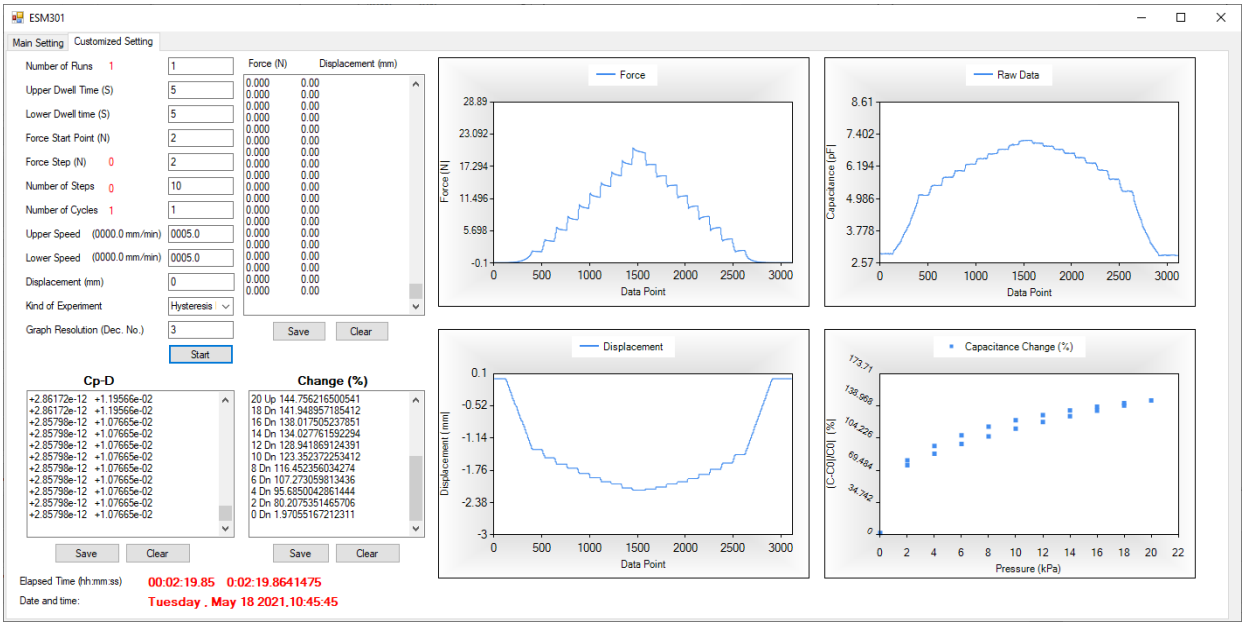

Figure 4.9. Hysteresis test settings and results.

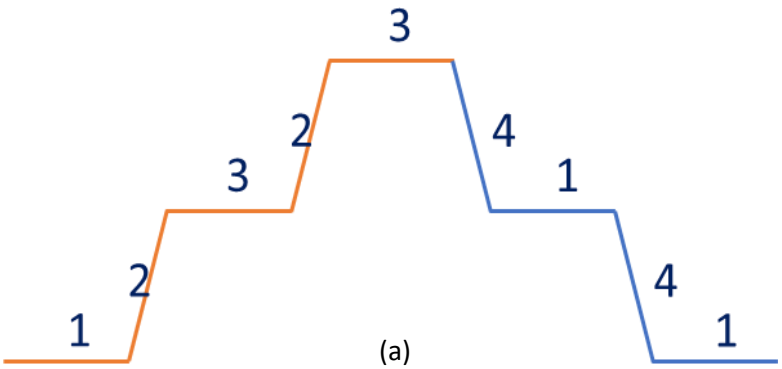

(a)

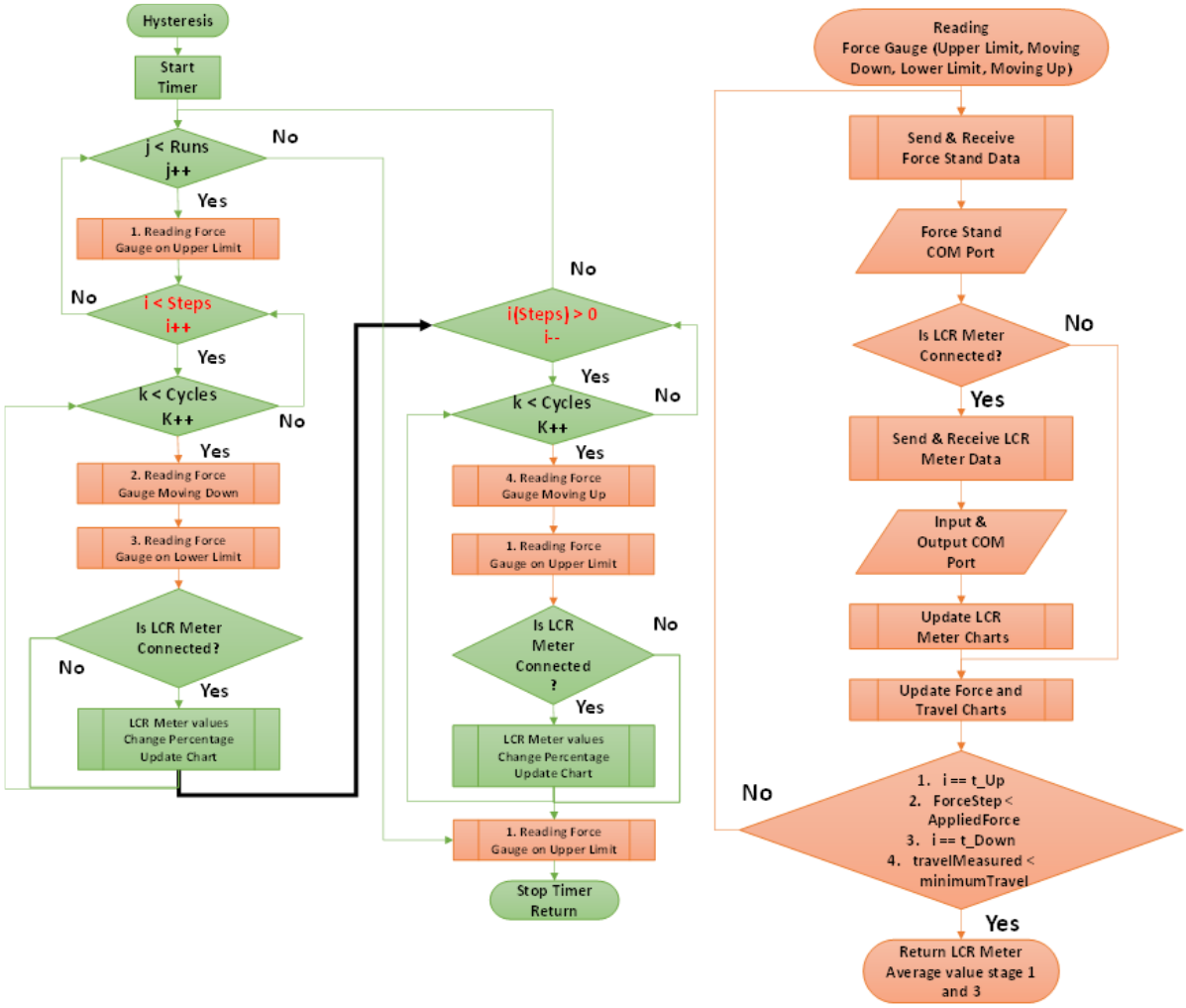

(b)

Figure 4.10. Hysteresis test , (a) stages, (b) flowchart.

and LCR meter values are also read in this function, when the applied force is bigger than the force set point, the loop will break, and force gauge will stop at this point. Then, in stage three, the program calls function three to read and return raw data and the average LCR meter value. The updating loop will experience a break when the specified time is over. Next, when the timer stopped at stage three, the force gauge calls related function and moves down again and will stop at next force set point. This process will be repeated for each step in the loop. When the force step reaches the last set point, the applied force is decreased step by step. To have a symmetric graph, the read function from first stage will be called again and then the stopwatch is paused. On downward trend, related functions in stage four and one will be called in each cycle and the average value on first stage will be used to calculate the capacitance change. The number of functions on Fig. 4.10 shows the stages on this experiment.

4.3. Development of a Software Program to Control Multi-Channel Flow Ratio/Pressure Controller Type 647C

To deliver the gas or air flow to the sensor, a gas system with controlled channels is essential. In this section, the fabrication process of a reliable gas delivery system as well as the development of a software for controlling the flow of gas in different channels are explained.

4.3.1. Fabrication of Gas Delivery System

The gas delivery system was designed in AutoCAD and assembled by using tubes, pipes, valves, chamber, and gas flow controllers. Figure 4.11 shows the schematic and AutoCAD design of the fabricated gas system. To control the flow of gas in this system, a customized C# program was developed for characterizing sensors and performing hysteresis, durability, and repeatability tests. To record the electrical responses of a sensor, a software was developed to control and

record the data from the gas controller and LCR meter. In addition, the software can analyze data simultaneously and show the sensitivity of the sensor in each cycle. The ambient air was used to investigate the performance of the gas system in terms of leakage. In the designed software, the accuracy of the gas flow controlling system was demonstrated by measuring, displaying, and recording the flow of the four channels using textboxes and graphs. As shown in Figure 4.12, stainless steel pipes and valves were used in the fabrication of this gas system to protect them when exposed to different chemical gases. Three flow channels are reserved for an input gas, and an isolated airtight chamber box is available with an access to the sensors and its wires so that the sensors can be connected to the LCR meter externally.

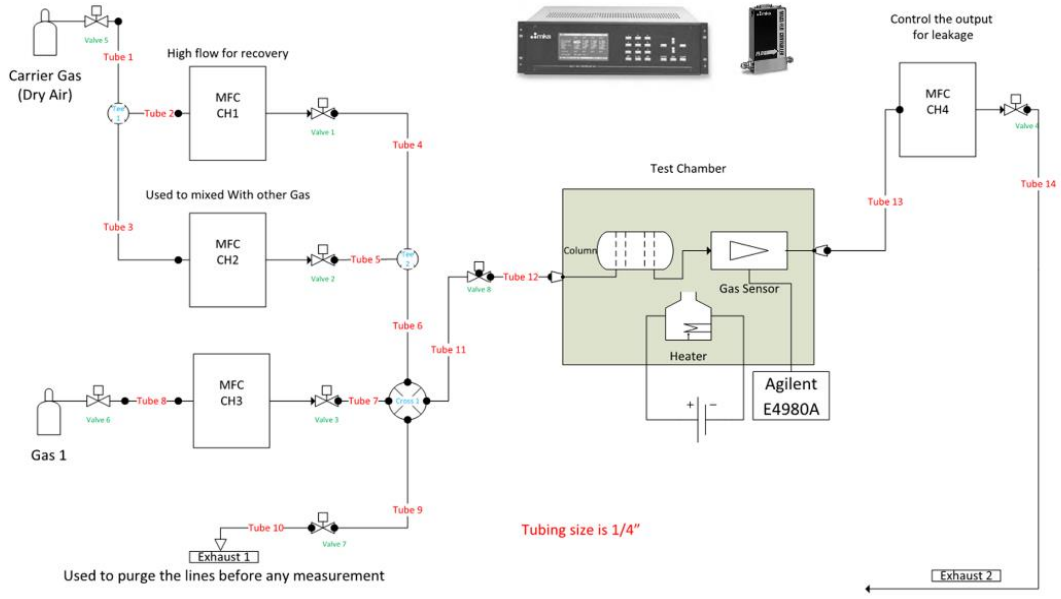

(a)

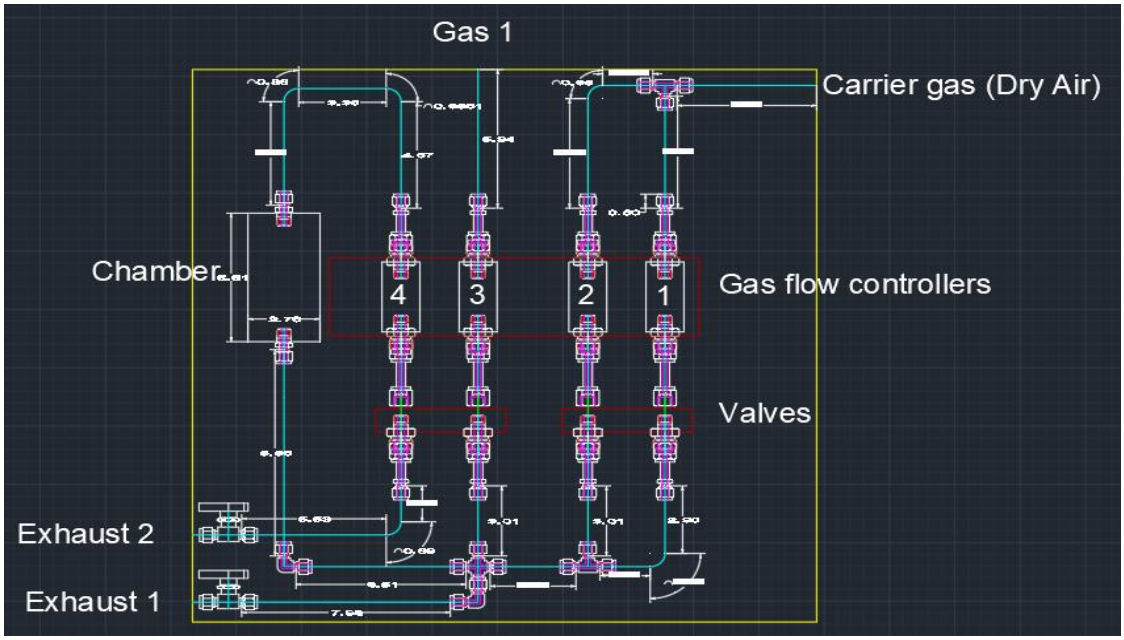

(b)

Figure 4.11. Gas system layout (a) schematic and, (b) AutoCAD design.

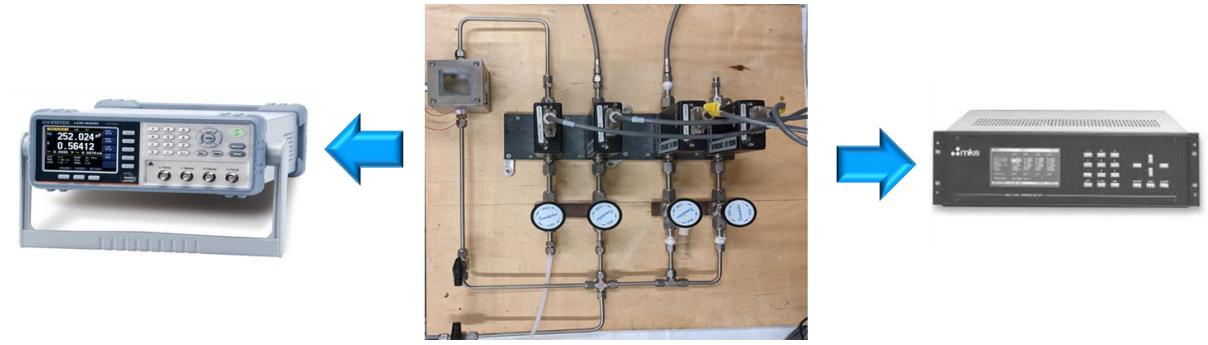

Figure 4.12. Fabricated gas system, (a) Instek LCR meter-6100, (b) gas delivery system, (c) Multi-Channel Flow Ratio/Pressure Controller Type 647C.

4.3.2. Software for Multi-Channel Flow Ratio/Pressure Controller Type 647C

Figure 4.13 shows the flowchart of the software developed to control the three channel flows and record their flows as well as LCR meter values. Initially, the program interface will be loaded with the tabs labelled as “Main Settings” and “Customized Settings”. All the available COM ports will be visible and the communication to a machine can be initiated by selecting the corresponding COM port. The “Read Settings” function will acquire and read the settings of LCR meter. In “Main Settings” of Fig 4.14, various settings such as gas range, correction factor, channel mode, high/low limit, etc. can be varied.

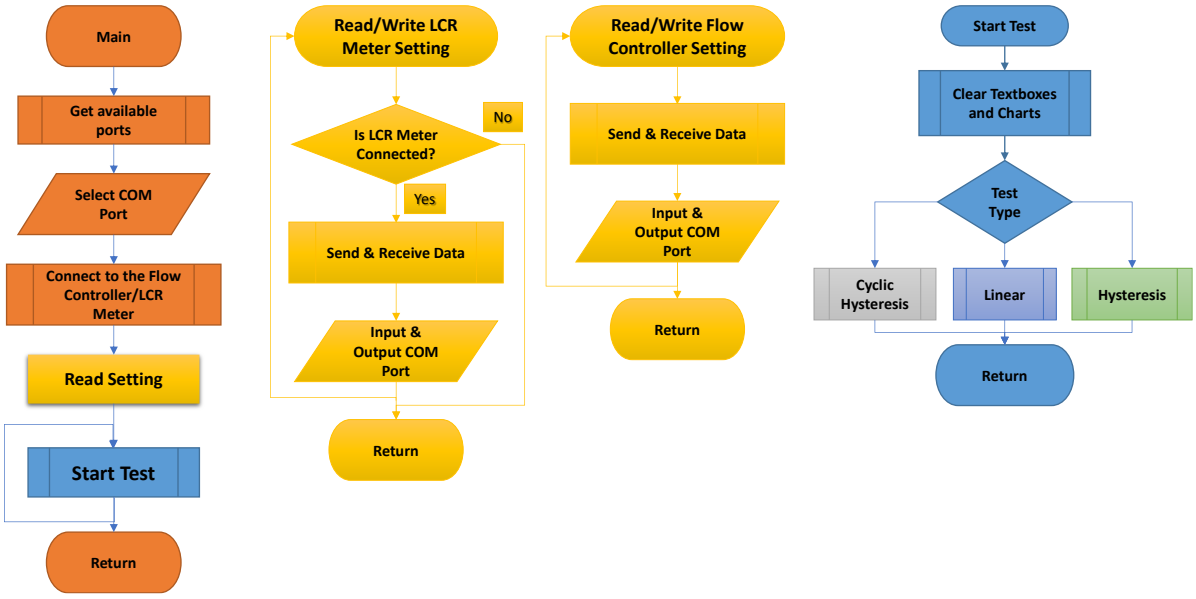

Figure 4.13. Main flowcharts.

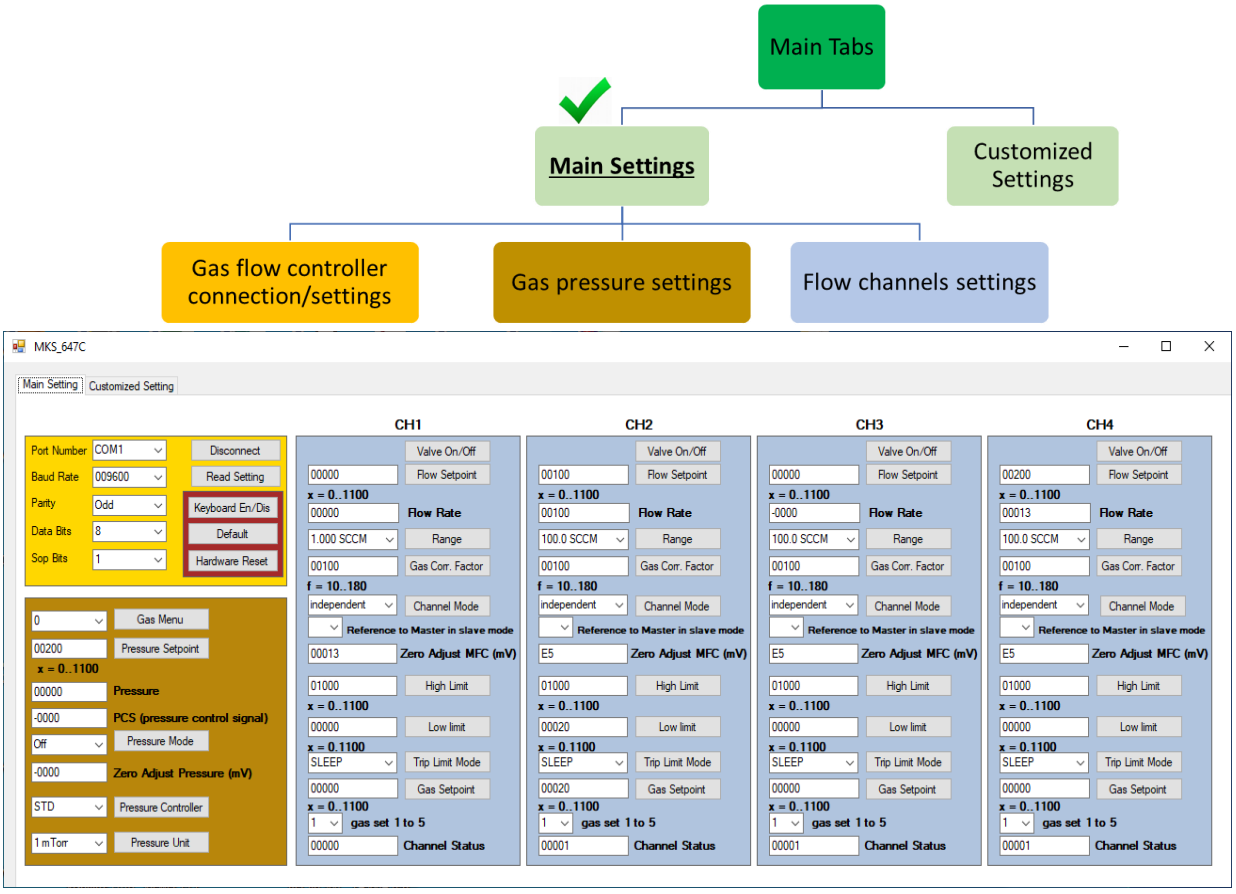

Figure 4.14. Main settings page.

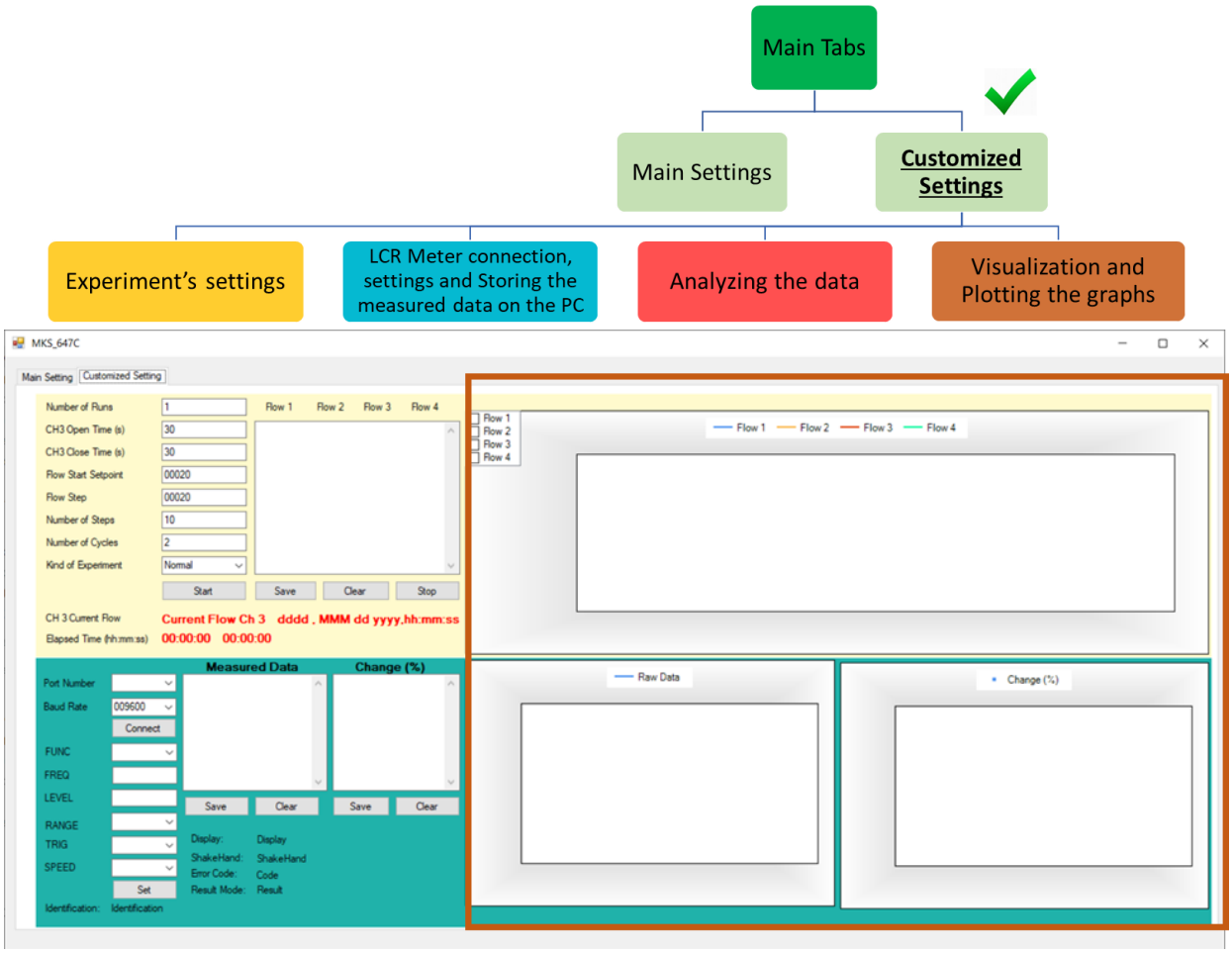

Figure 4.15. Customized settings page.

After connecting to the gas controller and verifying all the settings, the test can be started (Fig. 4.15) for performing various types of experiments involving multiple cycles of linear/exponential gas flow with different concentrations. Based on the gas availability, gas flow chart can be activated or disactivated to show the desirable graph. In customize setting tab, LCR meter connection panel is available and can be connected to the device by selecting the COM port. When it is connected, settings includes frequency, function, level, range, and speed of recording can be shown on text boxes. Accordingly, if sensor is available in the chamber, raw data and percentage change of values recorded by LCR meter could be shown on textboxes and charts. linear and cyclic hysteresis test example results are shown in Fig. 4.16(a,b), respectively.

In this experiment, channel one was closed, channel two was used for carrying reference gas and channel three was used to provide other gases subjected for testing.

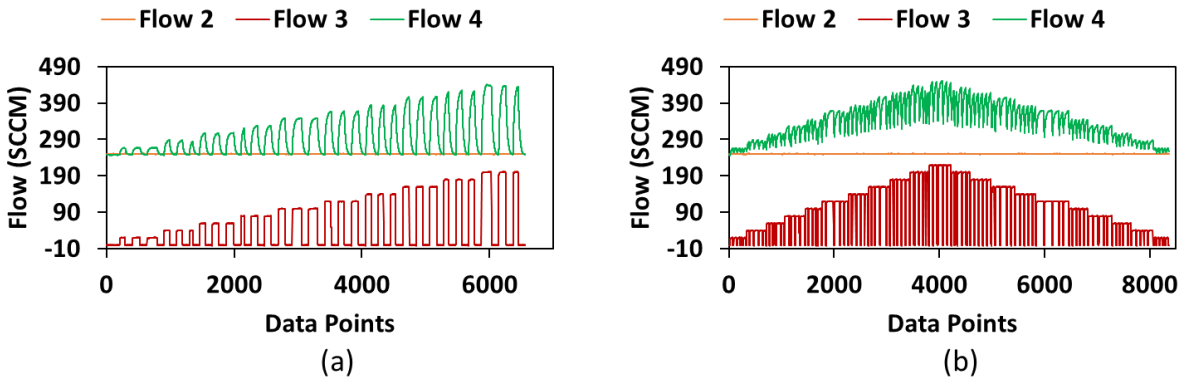

Figure 4.16. Test type(a) linear and (b) hysteresis results.

4.3.2.1. Linear Test

When the experiment type is selected as a linear test, the test will run by pressing the start button as shown in Fig. 4.17. The timer and date help to find the exact sampling rate in each experiment.

Based on the flowchart shown in Fig. 4.18, after pressing the start button, the stopwatch function will start, and the compiler run the first cycle from the flow set point. For each cycle, in

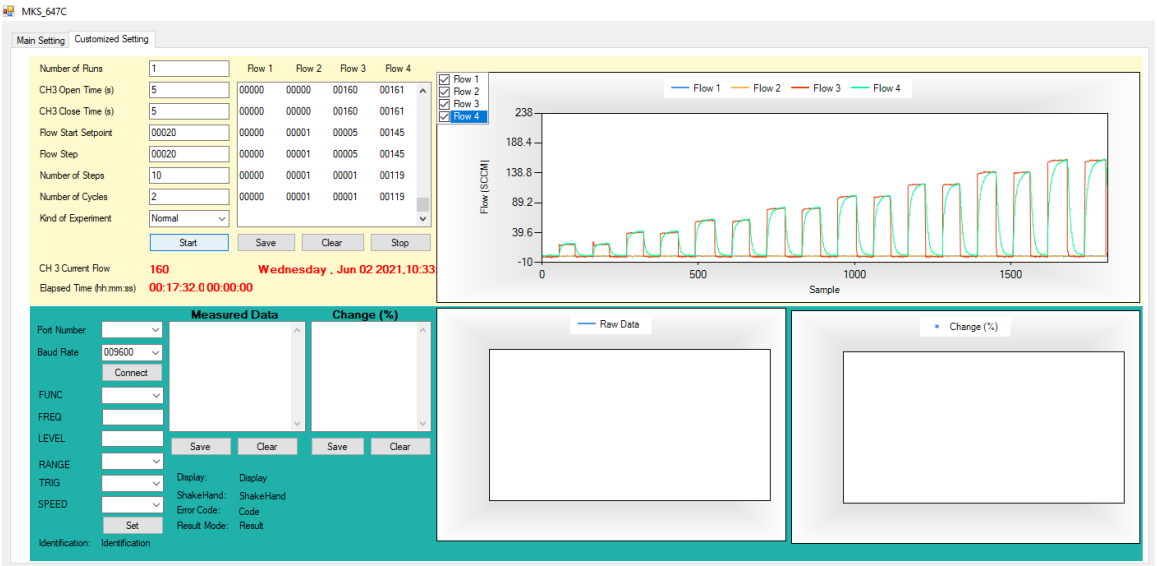

Figure 4.17. Normal test settings and results.

stage one, flow of channel three measured when the valve is closed by calling related function in stage one that can write commands to the gas system and read its response. If LCR meter is connected, this function can return the measured average capacitance value. The LCR meter raw data and flow charts will be dynamically updated in real-time. The loop will break when the set time gets completed . In stage two, the software sends the command to the gas system to close valve of channel three at defined setpoint. Flow and LCR meter values will be recorded by using function two and when the flow of channel three is higher than the setpoint, the loop will break, and valve will open at this flow point. Next, it calls function three to read and return the average LCR meter value. The loop will break when the set time is over. In stage four, channel three will be closed and the data will be recorded by calling function four. During these four stages, charts will be updated in real time. When the compiler goes back to the main linear function, capacitance change will be calculated based on two values from stage one and three. This process will be repeated for each cycle in loop.

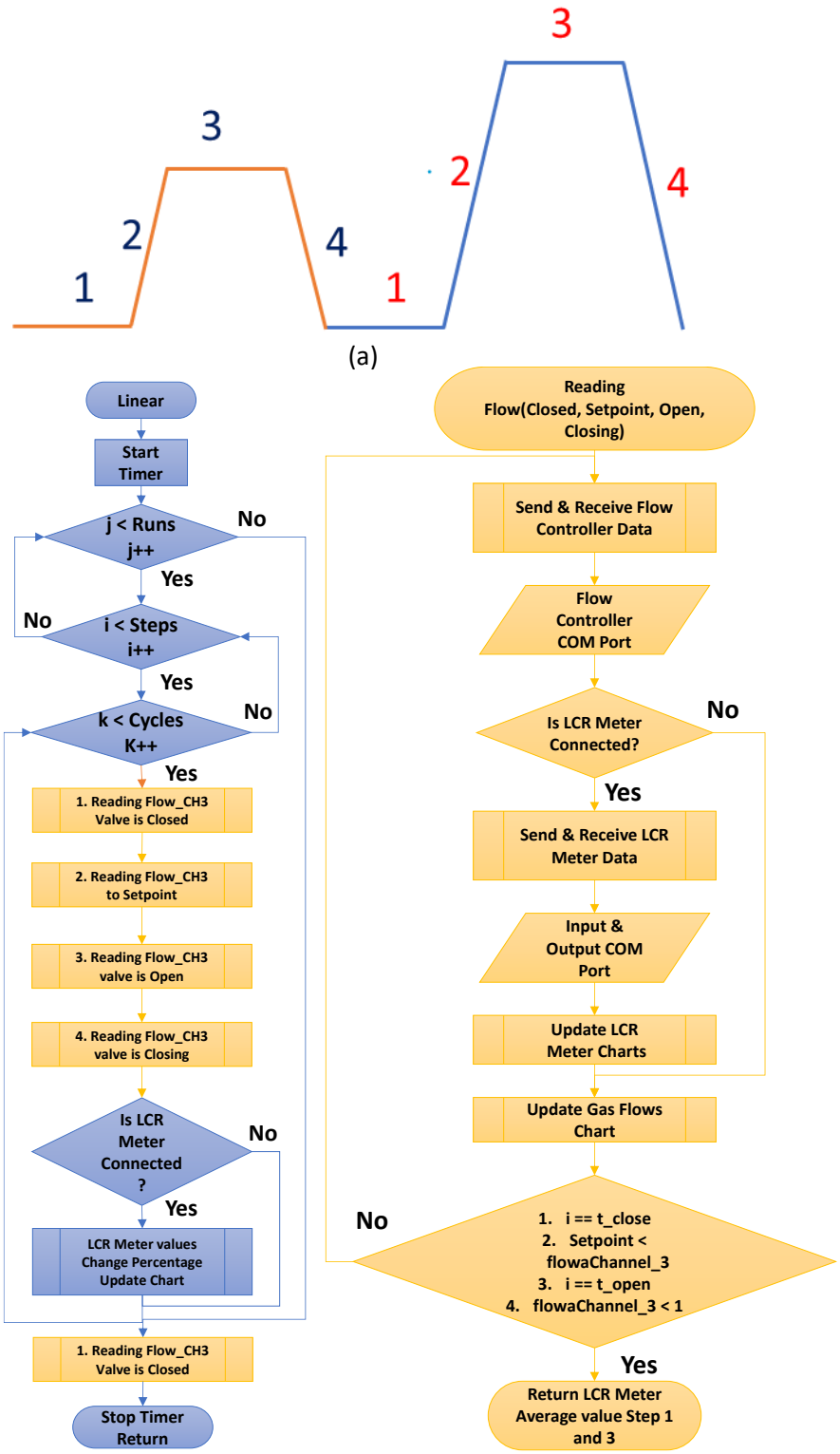

Figure 4.18. Normal test , (a) stages, (b) flowchart.

4.3.2.2. Cyclic Hysteresis Test

By selecting the cyclic hysteresis test and pressing the start button, the test can be performed based on the settings on “Customizations” tab. The save button provides the capability to save logged data to a text file for more data processing. The stopwatch can help to calculate the sampling rate based on the number of samples divided by the elapsed time. Figure 4. 19 shows the cyclic hysteresis test and its setting as well as the results. There are four checkboxes next to the chart that the operator can select to achieve desirable flow graph.

Based on flowchart of Fig. 4.20, after pressing the start button, stopwatch will start, and the compiler run the first cycle from the set force step . For each cycle, in stage one, flow of channel three will be read when it is stopped by calling a function that can write commands to gas flow controller. If LCR meter is connected, this function can return the average of measured values. The LCR meter raw data, and flow charts will be updated continuously. The loop will break when the set time is over. Next, the software sends the command to the gas flow controller to open the valve. Flow and LCR meter values will be read in function two and when the flow of channel three is higher than the flow set point, the loop will break, and flow controller will open the valve with the same set point and calls the function three to read and return the average LCR meter

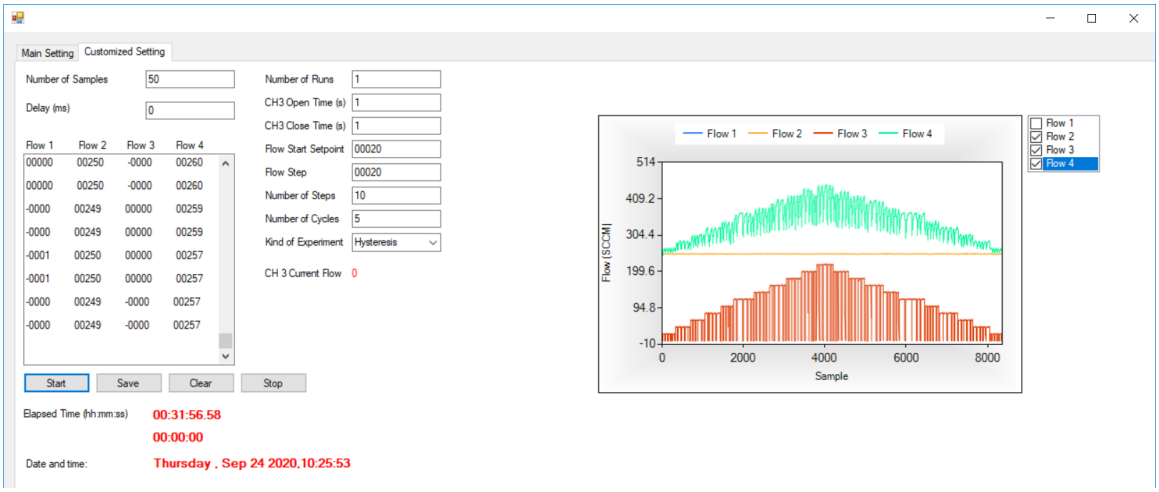

Figure 4.19. Cyclic hysteresis test settings and results.

value. The loop will break when the specified time is over. In stage four, flow controller will close the valve of channel three and the related function in stage four, to read the values until the stop function. When the compiler return to the main function, The changes in the measured values of LCR meter will be calculated based on two values from step one and three. This process will be repeated for each cycle in loop. When it reaches to the last step, it is time to follow step by step reduction in the gas flow.

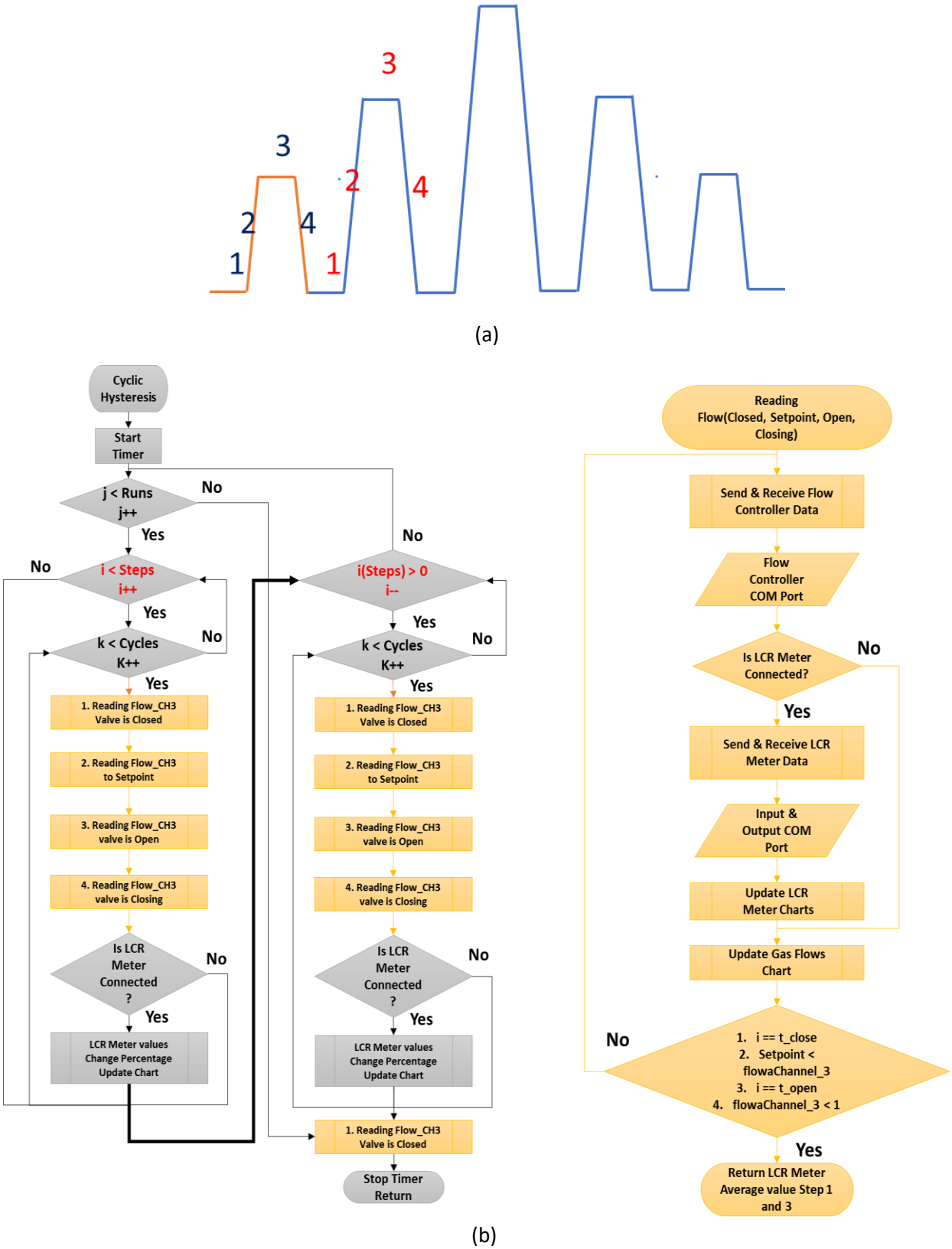

Figure 4.20. Cyclic hysteresis , (a) stages, (b) flowchart.

4.4. Summary

In this chapter, two software programs were successfully developed to perform reliable and repeatable experiment setups for pressure sensing and gas sensing systems. The developed software facilitates automatic control of the experiments which will reduce the human interference during the experiments and data collection. This results in the reduction of human errors which has remained unavoidable even when well trained technicians are employed. Various experiments including dynamic and static tests, cyclic tests, hysteresis tests were designed and their functionality was explained using the relevant flowcharts. An overview of the assembly of the gas delivery system was introduced with their corresponding schematics and the AutoCAD designs. Both pressure and gas flow controller software were developed in Visual Studio, C# language. The developed software enables the capability of performing various experiments and making big data sets which is envisioned to be very helpful for the machine learning purposes. In the following chapter, the author concludes this thesis by providing a summary of the performed projects along with some suggestions for the future work.

CHAPTER V

CONCLUSION AND FUTURE WORK

5.1. Conclusion

In the first project, a novel highly sensitive cone structured porous polydimethylsiloxane (PDMS) based pressure sensor capable of detecting very low-pressure ranges was developed for wearable respiration monitoring applications. The pressure sensor was fabricated using a master mold, a dielectric layer and fabric-based electrodes. The master mold with inverted cone structures was created using a rapid and precise three-dimensional (3D) printing technique. The dielectric layer with a porous and cone structures was prepared by annealing the mixture of PDMS, nitric acid (HNO3) and sodium bicarbonate (NaHCO3) in a master mold with inverted cone structures. The electrodes were developed by screen printing silver on fabric. A sensitivity of ≈530 %kPa-1 was measured for the fabricated pressure sensor at ultra-low-pressure ranges from 0 Pa to 10 Pa. The porous-cone structures provided an excellent deformation and thus resulted in high sensitivity for detecting very low-pressure ranges below 100 Pa. As an application demonstration, the pressure sensor was sewed inside a surgical mask and its capability to detect different respiration rates (normal, fast, and deep breathes) was investigated. An airflow controller system, custom-built software, and readout circuit was also developed for performing the continuous sensor data acquisition and capacitance conversions while changing the airflow rate.

In the second project, two software programs were successfully developed for controlling a pressure sensing and gas sensing system. The goal of this project was to help reducing the measurements errors associated with human interferences when testing pressure sensors and gas flow sensors. The developed software provided a reliable data collection pathway with controlled experiment setup under the application of multiple cycles of the stimulus. The sensor lifetime can

also be extracted by examining it under the application of continuous and uniform amounts of the corresponding stimulus, which can be applied in practical applications such as health monitoring devices. The related flowcharts, and processes of the main functions were also discussed.

5.2. Future Work

The author believes that the obtained results can be improved by addressing a few issues. Some suggestions for the future work are discussed below.

Cone-Structured Porous Capacitive Pressure Sensor for Wearable Health Monitoring:

- Establishing a correlation among the respiration rate of human, airflow in the chamber and capacitance measurements of the sensor.
- Investigation of the various pore sizes on the sensitivity of the cone-structured porous pressure sensors.
- Fatigue testing and analysis of micro-pyramid structures are required to know the maximum mechanical bending, compression, and deformation of the micro-pyramid structures.
- Investigation of various aspect ratio of cone structures to optimize the sensitives of the pressure sensors for wide pressure ranges.

Software Development:

- Adding more features and types of analysis to the software such as Young's Modulus, and compressive Modulus measurements.
- Improving the graphical interface/visualization of the plotted graphs such as adding the capability to change the color, size, or visibility of the graphs when the user interacts with them.

REFERENCES

[1] Lu, D. H Kim, “Flexible and stretchable electronics paving the way for soft robotics,” Soft Robotics vol. 1(1), pp. 53-62, 2014.

[2] R. Lin et al. “Paper/carbon nanotube-based wearable pressure sensor for physiological signal acquisition and soft robotic skin,” ACS applied materials & interfaces, vol. 9(43), pp. 37921-37928, 2017.

[3] G. Kim et al. “Transparent, flexible, conformal capacitive pressure sensors with nanoparticles,” Small, vol. 14(8), pp.1703432, 2018.

[4] V. Palaniappan, S. Masihi, M. Panahi, D. Maddipatla, A. K. Bose, X. Zhang, B. B. Narakathu, B. J. Bazuin, M. Z. Atashbar, “Laser-assisted fabrication of a highly sensitive and flexible micro pyramid-structured pressure sensor for E-Skin applications,” IEEE Sensors Journal, vol. 20 (14), pp. 7605-7613, 2020.

[5] J. Park, M. Kim, Y. Lee, H. S. Lee and H. Ko, “Fingertip skin–inspired microstructured ferroelectric skins discriminate static/dynamic pressure and temperature stimuli,” Sci. Adv, vol. 1 (9), pp. 1500661, 2015.

[6] S. Masihi et al, "Development of a flexible tunable and compact microstrip antenna via laser assisted patterning of copper film," IEEE Sens. J., vol. 20 (14), pp.7579 - 7587, 2020.

[7] S. Masihi, P. Rezaei and M. Panahi, “Compact chip-resistor loaded active integrated patch antenna for ISM band applications,” Wireless Pers. Commun., vol. 97 (4), pp. 5733–5746, 2017.

[8] A. D. Santos et al, “Piezoresistive E-skin sensors produced with laser engraved molds,” Adv. Electron Mater., vol. 4 (9), pp. 1800182, 2018.

[9] A. A. Chlaihawi, B. B. Narakathu, S. Emamian, B. J. Bazuin and M. Z. Atashbar, “Development of printed and flexible dry ECG electrodes,” Sens. Biosensing Res., vol. 20, pp. 9-15, 2018.

[10] Yu, Guohui, Jingdong Hu, Jianping Tan, Yang Gao, Yongfeng Lu, and Fuzhen Xuan. "A wearable pressure sensor based on ultra-violet/ozone microstructured carbon nanotube/polydimethylsiloxane arrays for electronic skins." Nanotechnology, vol. 29(11), p.115502, 2018.

[11] S. Ali et al, “Flexible capacitive pressure sensor based on PDMS substrate and Ga-In liquid metal,” IEEE Sens. Journal vol. 19, pp. 97-104, 2019.

[12] A. Moorthi; B. B. Narakathu, A. S. G. Reddy, A. Eshkeiti, H. Bohra and M. Z. Atashbar, “A novel flexible strain gauge sensor fabricated using screen printing,” IEEE Sens., pp. 765-768, 2012, doi: 10.1109/ICSensT.2012.6461780.

[13] R. Punj, R. Kumar, “Technological aspects of WBANs for health monitoring:a comprehensive review,” Wireless Networks, 25:1125–1157, 2019.

[14] A. Rahaman et. al., “Developing IoT Based Smart Health Monitoring Systems: A Review,” Vol. 33, No. 6, pp. 435-440, 2019.

[15] S. D. Bersch et. al., “Sensor data acquisition and processing parameters for human activity classification ,” Sensors, 14, 4239-4270, 2014.

[16] M. M. Baig et. al., “A systematic review of wearable patient monitoring systems – current challenges and opportunities for clinical adoption,” J Med Syst, 41: 115, 2017.

[17] I. M. Pires et. al., “From data acquisition to data fusion: a comprehensive review and a roadmap for the identification of activities of daily living using mobile devices,” Sensors, 16, 184, 2016.

[18] H. H. Nguyen, F. Mirza, M. A. Naeem and M. Nguyen, "A review on iot healthcare monitoring applications and a vision for transforming sensor data into real-time clinical feedback," Proceedings of the 2017 IEEE 21st International Conference on Computer Supported Cooperative Work in Design (CSCWD), 2017.

[19] US Centers for Disease Control and Prevention. Coronavirus disease 2019 (COVID-19) data tracker. Accessed July 2, 2021. https://covid.cdc.gov/covid-data-tracker/#cases_casesinlast7days.

[20] M. Nemati, J. Ansary, N. Nemati, "Machine learning approaches in COVID-19 survival analysis and discharge time likelihood prediction using clinical data," Patterns, Patter 100074, 2020.

[21] F. Li, M. Valero, H. Shahriar, R. A. Khan, S. I. Ahamed, "Wi-COVID: A COVID-19 symptom detection and patient monitoring framework using WiFi," Smart Health, vol. 19, 100147, 2021.

[22] S. Richardson et al, "Presenting characteristics, comorbidities, and outcomes among 5700 patients hospitalized with COVID-19 in the New York city area," JAMA, 323(20):2052-2059, 2020.

[23] Z. Imam et al, "Older age and comorbidity are independent mortalitypredictors in a large cohort of 1305 COVID-19 patients inMichigan, United States," J Intern Med, 288(4):469-476, 2020.

[24] R. Ghosh et al, "Fabrication of piezoresistive Si nanorod-based pressure sensor arrays: A promising candidate for portable breath monitoring devices," Nano Energy, vol. 80, 105537, 2021.

[25] A. M. Baig, “Computing the effects of SARS-CoV-2 on respiration regulatory mechanisms in COVID-19,” ACS Chemical Neuroscience 11 (16), , 2416-2421, 2020.

[26] Z. Zhou et al. “Supersensitive all-fabric pressure sensors using printed textile electrode arrays for human motion monitoring and human–machine interaction,” Journal of Materials Chemistry C, vol. 6(48), pp. 13120-13127, 2018.

[27] M. Chatopadhyay, D. Charkraborty, “A new scheme for determination of respiration rate in human being using MEMS based capacitive pressure sensor: simulation study,” in Proceedings of the 8th International Conference on Sensing Technology, 2-4 Sep. 2014, Liverpool, UK, pp. 236-240.

[28] S. Chen et al. “Noncontact heartbeat and respiration monitoring based on a hollow microstructured self-powered pressure sensor,” ACS Appl. Mater. & inter., vol. 10(4), pp. 3660-3667, 2018.

[29] S. Sharma et al. “Wearable capacitive pressure sensor based on MXene composite nanofibrous scaffolds for reliable human physiological signal acquisition,” ACS Appl. Mater. & Inter., 2020.

[30] Sight, Sound, Smell, Taste, and Touch: How the Human Body Receives Sensory Information. Accessed July 14, 2021. https://www.visiblebody.com/learn/nervous/five-senses.

[31] A. K. Bose, X. Zhang, D. Maddipatla, S. Masihi, M. Panahi, B. B. Narakathu, B. J. Bazuin, J. D. Williams, M. F. Mitchell, M. Z. Atashbar, “Screen-printed strain gauge for micro-strain detection applications,” IEEE Sensors Journal, vol. 20(21), pp. 12652 – 12660, 2020. DOI: 10.1109/JSEN.2020.3002388

[32] X. Zhang, D. Maddipatla, A. K. Bose, B. B. Narakathu, M. Z. Atashbar, “Effect of excitation signal frequency on the electrical response of a MWCNT/HEC composite based humidity sensor,” IEEE Sensors Conference, 2020. (Accepted).

[33] M. Z. Atashbar, H. T. Sun, B. Gong, W. Wlodarski, R. Lamb, “XPS study of Nb-doped oxygen sensing TiO2 thin films prepared by sol-gel method,” Thin Solid Films, vol. 326(1-2), pp. 238-244, 1998. DOI: 10.1016/S0040-6090(98)00534-3.

[34] Z. Ramshani, A. S. G. Reddy, B. B. Narakathu, M. Z. Atashbar, “SH-SAW sensor based microfluidic system for the detection of heavy metal compounds in liquid environments,” Sens. Actuators B Chem., vol. 217(1), pp. 72-77, 2015.

[35] B. B. Narakathu, W. Guo, S. O. Obare, M. Z. Atashbar, “Novel approach for detection of toxic organophosphorus compounds,” Sens. Actuators B Chem., vol. 158, pp. 69-74, 2011.

[36] M. Z. Atashbar, B. Bejcek, S. Singamaneni, S. Santucci, “Carbon nanotube based biosensors,” Proc. of IEEE Sensors, pp. 1048-1051 vol. 2, 2004. DOI: 10.1109/ICSENS.2004.1426354

[37] D. Maddipatla, B, B. Narakathu, B. J. Bazuin, M. Z. Atashbar, “Development of a printed impedance based electrochemical sensor on paper substrate,” Proc. of IEEE Sensors, pp. 1-3, 2016. DOI: 10.1109/ICSENS.2016.7808785

[38] B. B. Narakathu, M. Z. Atashbar, B. Bejcek, “Pico-mole level detection of toxic bio/chemical species using impedance based electrochemical biosensors,” Sensor Letters, vol. 9(2), pp. 872-875, 2011. DOI: 10.1166/sl.2011.1634.

[39] M. Z. Atashbar, V. Bliznyuk, D. Banerji, S. Singamaneni, “Deposition of parallel arrays of palladium nanowires on highly oriented pyrolytic graphite,” Journal of alloys and compounds, vol. 372(1-2), pp. 107-110, 2004. DOI: 10.1016/j.jallcom.2003.10.014.

[40] A. Eshkeiti et al, “A stretchable and wearable printed sensor for human body motion monitoring,” IEEE Sensors Proceedings, pp. 1-4, 2015. DOI: 10.1109/ICSENS.2015.7370412.

[41] S. Krishnamurthy, B. J. Bazuin, M. Z. Atashbar, “Wireless SAW sensors reader: architecture and design,”. IEEE International Conference on Electro Information Technology Proceedings, pp. 6, 2005. DOI: 10.1109/EIT.2005.1626992.

[42] M. Z. Atashbar, “Nano-sized TiO/sub 2/thin film for alcohol sensing application,” IEEE Conference on Nanotechnology Proceedings, pp. 544-549, 2001. DOI: 10.1109/NANO.2001.966482.

[43] M. Z. Atashbar, W. Wlodarski, “Design, simulation and fabrication of doped TiO2-coated surface acoustic wave oxygen sensor,” Journal of intelligent material systems and structures, vol. 8(11), pp. 953-959, 1997. DOI: 10.1177/1045389X9700801104.

[44] M. Z. Atashbar, D. Banerji, S. Singamaneni, V. Bliznyuk, “Polystyrene palladium nanocomposite for hydrogen sensing,” Molecular Crystals and Liquid Crystals, vol. 427(1), pp. 217-529, 2005. DOI: 10.1080/15421400590892299.

[45] M. Z. Atashbar, S. Krishnamurthy, G. Korotcenkov, “Basic principles of chemical sensor operation,” Chemical Sensors: Fundamentals of Sensing Materials, vol, 1, pp. 1-62, 2010.

[46] M. Z. Atashbar et al, “Palladium nanowire hydrogen sensor based on a SAW transducer,” IEEE Sensors Proceedings, pp. 3, 2005. DOI: 10.1109/ICSENS.2005.1597961.

[47] C. J. Cheng, C. T. Feng, M. Z. Atashbar, “The analysis of IgG-protein a binding effect by quartz crystal microbalance biosensor,” IEEE Sensors Proceedings, pp. 228-231, 2010. DOI: 10.1109/ICSENS.2010.5690442.

[48] B. B. Narakathu, B. E. Bejcek, M. Z. Atashbar, “Improved detection limits of toxic biochemical species based on impedance measurements in electrochemical biosensors,” Biosensors and Bioelectronics, vol. 26, pp. 923-928, 2010.

[49] V. S. Turkani, D. Maddipatla, B. B. Narakathu, B. J. Bazuin, M. Z. Atashbar, “A carbon nanotube based NTC thermistor using additive print manufacturing processes,” Sensors and Actuators A: Physical, vol. 279, pp.1-9, 2018.

[50] A. Eshkeiti, B. B. Narakathu, A. S. G. Reddy, A. Moorthi, M. Z. Atashbar, E. Rebrosova, M. Rebros and M. Joyce, “Detection of heavy metal compounds using a novel inkjet printed surface enhanced raman spectroscopy (SERS) substrate,” Sens. Actuator B-Chem., vol. 171, pp. 705–711, 2012.

[51] M. Ochoa, R. Rahimi, J. Zhou, H. Jiang, C. K. Yoon, M. Oscai, V. Jain, T. Morken, R. H. Oliveira, D. Maddipatla, B. B. Narakathu, et al, “A manufacturable smart dressing with oxygen delivery and sensing capability for chronic wound management,” In Micro-and Nanotechnology Sensors, Systems, and Applications X, vol. 10639, pp. 106391C, 2018.

[52] B. B Narakathu, S. G. R.Avuthu, A. Eshkeiti, S. Emamian, and M. Z. Atashbar, “Development of a microfluidic sensing platform by integrating PCB technology and inkjet printing process,” IEEE Sens. J. 15, 6374–6380 (2015).

[53] D. Maddipatla, F. Aljanabi, B.B. Narakathu, M.M. Ali, V.S. Turkani, B.J. Bazuin, P.D. Fleming, M.Z. Atashbar, “Development of a novel wrinkle-structure based SERS substrate for drug detection applications” Sensing and Bio-Sensing Research vol. 24, 100281-7, 2019. DOI: 10.1016/j.sbsr.2019.100281

[54] A. Eshkeiti, M. Rezaei, B. B. Narakathu, A. S. G. Reddy, M. Z. Atashbar, “Gravure printed paper based substrate for detection of heavy metals using surface enhanced Raman

spectroscopy, SERS", IEEE Sensors Conference, pp.667-674, 2013. DOI: 10.1109/ICSENS.2013.6688292.

[55] S. Emamian, A. A. Chlaihawi, B.B. Narakathu, B.J. Bazuin, M.Z. Atashbar, "A piezoelectric based vibration energy harvester fabricated using screen printing technique", 15th IEEE Sensors Conference, pp. 485-487, 2016. DOI: 10.1109/ICSENS.2016.7808560.

[56] S. Emamian, A.A. Chlaihawi, B.B. Narakathu, M.Z. Atashbar, "Fabrication and characterization of piezoelectric paper based device for touch and force sensing applications", 30th Eurosensors Conference, pp. 1786-1789, 2016. DOI: 10.1016/j.proeng.2016.11.248

[57] A.A. Chlaihawi, B.B. Narakathu, A. Eshkeiti, S. Emamian, A.S.G. Reddy, M.Z. Atashbar, "Screen printed MWCNT/PDMS based dry electrode sensor for electrocardiogram (ECG) measurements", IEEE International Conference on Electro/Information Technology, EIT, pp. 526-529, 2015. DOI: 10.1109/EIT.2015.7293392.

[58] S. Hajian et al., "Development of a fluorinated graphene-based resistive humidity sensor", IEEE Sensors Journal, vol. 20(14), pp. 7517-7524, 2020. DOI: 10.1109/JSEN.2020.2985055.

[59] S. Masihi, M. Panahi, S. Hajian, D. Maddipatla, S. Ali, X. Zhang, A. K. Bose, B. B. Narakathu, B. J. Bazuin, M. Z. Atashbar, "A highly sensitive capacitive based dual-axis accelerometer for wearable applications", IEEE EIT Conference, 2020.

[60] V. Palaniappan, D. Maddipatla, M. Panahi, S. Masihi, A. K. Bose, X. Zhang, S. Hajian, Binu B. Narakathu, B. J. Bazuin, M. Z. Atashbar, "Highly sensitive and flexible M-Tooth based hybrid micro-structured capacitive pressure sensor," IEEE FLEPS Conference, 2020.

[61] X. Zhang, A. K. Bose, D. Madipatla, S. Masihi, V. Palaniappan, M. Panahi, B. B. Narakathu, M. Z. Atashbar, "Development of a novel and flexible MWCNT/PDMS based resistive force sensor," IEEE FLEPS Conference, 2020.

[62] A. K. Bose, D. Maddipatla, X. Zhang, M. Panahi, S. Masihi, B. B. Narakathu, B. J. Bazuin, M. Z. Atashbar, “Screen printed silver/carbon composite strain gauge on a TPU platform for wearable applications”, IEEE FLEPS Conference, 2020. DOI: 10.1109/FLEPS49123.2020.9239547.

[63] G. R Avuthu et al, “Development of screen printed electrochemical sensors for selective detection of heavy metals,” IEEE SENSORS Proceedings, pp. 1-4, 2015. DOI: DOI: 10.1109/ICSENS.2015.7370297.

[64] S. G. R Avuthu et al, “Detection of heavy metals using fully printed three electrode electrochemical sensor,” IEEE SENSORS Proceedings, pp. 669-672, 2014. DOI: 10.1109/ICSENS.2014.6985087.

[65] J. S. Wilson, “Sensor technology handbook,” Elsevier, 2004.

[66] B. N. Altay, J. Jourdan, V. S. Turkani, H. Dietsch, D. Maddipatla, A. Pekarovicova, P. D. Fleming, M. Z. Atashbar, “Impact of substrate and process on the electrical performance of screen-printed nickel electrodes: fundamental mechanism of ink film roughness,” ACS Applied Energy Materials, vol. 1(12), pp. 7164-7173, 2018.

[67] M. Ahmad, S. Malik, S. Dewan, A.K. Bose, D. Maddipatla, B.B. Narakathu, M.Z. Atashbar, M.S. Baghini, “An auto-calibrated resistive measurement system with low noise instrumentation ASIC,” IEEE Journal of Solid-State Circuits, vol. 55(11), pp. 3036–3050, 2020. DOI: 10.1109/JSSC.2020.3017639

[68] M. Ochoa, R. Rahimi, J. Zhou, H. Jiang, C.K. Yoon, D. Maddipatla, B.B. Narakathu, M. Oscai, V. Jain, T. Morken, R. H. Oliveira, G. L. Campana, M. A. Zieger, R. Sood, M. Z. Atashbar, B. Ziaie, “Integrated sensing and delivery of oxygen for next-generation smart wound dressings,” Nature Microsystems and Nanoengineering, vol. 6(1), pp. 1-16, 2020.

[69] T. Saeed, D. Maddipatla, B. B. Narakathu, S. O. Obare, M. Z. Atashbar, “Synthesis of a novel hexaazatriphenylene derivative for the selective detection of copper ions in aqueous solution,” RSC Advances, vol. 9(68), pp. 39824-39833, 2019.

[70] V.S. Turkani, D. Maddipatla, B.B. Narakathu, T. Saeed, S. O. Obare, B.J. Bazuin, M.Z. Atashbar, “A highly sensitive printed humidity sensor based on functionalized MWCNT/HEC composite for flexible electronics application”, Nanoscale Advances, vol. 1, pp. 2311-2322, 2019.

[71] S. Ali et al., “Flexible capacitive pressure sensor based on PDMS substrate and Ga–In liquid metal”, IEEE Sensors Journal, vol. 19(1), pp. 97-104, 2019. DOI: 10.1109/JSEN.2018.2877929.

[72] M. M. Ali et al., “Eutectic Ga-In liquid metal based flexible capacitive pressure sensor”, Proceedings of IEEE Sensors Conference, pp. 1-3, 2016. DOI: 10.1109/ICSENS.2016.7808515.

[73] S. Masihi, M. Panahi, B. Narakathu, B. Bazuin, M. Z. Atashbar “development of a flexible tunable and compact microstrip antenna via laser assisted patterning of copper film,” IEEE Sensors Journal, vol. 20, no. 14, pp. 7579-7587, 2020, doi: 10.1109/JSEN.2020.2987318.

[74] L. Bonek, S. Fenech, N. Sapoznik, A. J. Hanson, D. Maddipatla, M. Z. Atashbar, “Development of a flexible and wireless ECG monitoring device,” IEEE Sensors Conference, 2020. DOI: 10.1109/SENSORS47125.2020.9278904.

[75] G. Rius, A. Baldi, B. Ziaie, M. Z. Atashbar. "Introduction to micro-/nanofabrication." In Springer Handbook of Nanotechnology, pp. 51-86. Springer, Berlin, Heidelberg, 2017. DOI: 10.1007/978-3-662-54357-3_3.

[76] M. Joyce, P. D. Fleming III, S. G. Avuthu, S. Emamian, A. Eshkeiti, M. Atashbar, T. Donato, “Contribution of flexo process variables to fine line Ag electrode performance,” Int. J. Eng. Res. Technol, vol. 3(8), pp. 1645-1656, 2014.

[77] B. B. Narakathu, M. S. Devadas, A. S. G. Reddy, A. Eshkeiti, A. Moorthi, I. R. Fernando, B. Miller, G. Ramakrishna, E. Sinn, M. K. Joyce, M. Rebros, E. Rebrosova, G. Mezei, M. Z. Atashbar, “Novel fully screen printed flexible electrochemical sensor for the investigation of electron transfer between thiol functionalized viologen and gold clusters,” Sensors and Actuators B: Chemical, vol. 176, pp. 768-774, 2013.

[78] D. Maddipatla, B.B Narakathu,M. Ochoa, R. Rahimi, J. Zhou, C. Yoon, J. H. Chang; H. Al-Zubaidi, S. Obare, M. Zieger, B. Ziaie, M.Z. Atashbar “Rapid prototyping of a novel and flexible paper based oxygen sensing patch via additive inkjet printing process,” RSC Adv., 9, 22695-22704, 2019. DOI: 10.1039/C9RA02883H.

[79] X. Zhang, D. Maddipatla, A. K. Bose, B. B. Narakathu, M. Z. Atashbar, “A printed MWCNTs/PDMS based flexible resistive temperature detector,” IEEE EIT Conference, 2020. DOI: 10.1109/EIT48999.2020.9208334.

[80] X. Zhang, D. Maddipatla, A. K. Bose, S. Hajian, B. B. Narakathu, J. D. Williams, M. F. Mitchell, M. Z. Atashbar, “Novel printed carbon nanotubes based flexible resistive humidity sensor,” IEEE Sensors Journal, vol. 20(21), pp. 12592-12601, 2020, DOI: 10.1109/JSEN.2020.3002951.

[81] D. Maddipatla, B. B. Narakathu, S. G. R. Avuthu, S. Emamian, A. Eshkeiti, A.A. Chlaihawi, B. J. Bazuin, M. K. Joyce, C. W. Barrett, M. Z. Atashbar, “A novel flexographic printed strain gauge on paper platform,” 14th IEEE Sensors Conference, November 1-4, Busan, South Korea, 2015.

[82] S. Emamian, A. Eshkeiti, B. B. Narakathu, A. S. G. Reddy, M. Z. Atashbar, “Detection of 2,4-dinitrotoluene (DNT) using gravure printed surface enhancement Raman spectroscopy (SERS) flexible substrate,” IEEE Sensors Conference Proceedings, pp. 1069-1072, 2014. DOI: 10.1109/ICSENS.2014.6985189.

[83] S. G. R. Avuthu, B. B. Narakathu, M. Z. Atashbar, M. Rebros, E. Hrehorova, B. Bazuin, P. D. Fleming, M. K. Joyce, “Printed capacitive based humidity sensors on flexible substrates,” Sensor Letters, Vol. 9, 1–3, 2011. DOI: 10.1166/sl.2011.1633.

[84] V. S. Turkani et al., “Nickel based RTD fabricated via additive screen printing process for flexible electronics,” IEEE Access, vol. 7, pp. 37518-37527, 2019.

[85] D. Maddipatla, “Development of fully printed and flexible strain, pressure and electrochemical sensors,” Master's Theses, 750, Western Michigan University, 2016.

[86] V. S. Turkani, D. Maddipatla, B. B. Narakathu, B. J. Bazuin, M. Z. Atashbar, “A fully printed CNT based humidity sensor on flexible PET substrate”, 17th International Meeting on Chemical Sensors (IMCS), pp. 519-520, 2018. DOI: 10.5162/IMCS2018/P1FW.5.

[87] S. Emamian, A. Eshkeiti, B. B. Narakathu, S. G. R. Avuthu, M. Z. Atashbar, “Gravure printed flexible surface enhanced raman spectroscopy (SERS) substrate for detection of 2, 4-dinitrotoluene (DNT) vapor,” Sens. Actuator B-Chem., vol. 217, pp. 129-135, 2015.

[88] V. S. Turkani, D. Maddipatla, B. B. Narakathu, B. N. Altay, D. Fleming, B. J. Bazuin, M. Z. Atashbar, “A screen-printed nickel based resistance temperature detector (RTD) on thin ceramic substrate,” IEEE EIT Conference, 2020. DOI: 10.1109/EIT48999.2020.9208252.

[89] D. Maddipatla, X. Zhang, A. K. Bose, S. Masihi, B. B. Narakathu, B. J. Bazuin, M. Z. Atashbar, “Development of a flexible force sensor using additive print manufacturing

process," 2019 IEEE International Conference on Flexible and Printable Sensors and Systems (FLEPS), Glasgow, United Kingdom, 2019, pp. 1-3, doi: 10.1109/FLEPS.2019.8792307

[90] D. Maddipatla, T. Saeed, B. B. Narakathu, S. O. Obare, M. Z. Atashbar, "Incorporating a novel hexaazatriphenylene derivative to a flexible screen-printed electrochemical sensor for copper ion detection in water samples," IEEE Sensors Journal, vol. 20(21), pp. 12582 - 12591, 2020. DOI: 10.1109/JSEN.2020.3002811.

[91] M.M. Ali, D. Maddipatla, B.B Narakathu, A.A. Chlaihawi, S. Emamian, F. Janabi, B.J. Bazuin, M.Z. Atashbar "Printed strain sensor based on silver nanowire/silver flake composite on flexible and stretchable TPU substrate," Sensors and Actuators A: Physical, vol. 274, pp. 109-115, 2018. DOI: 10.1016/j.sna.2018.03.003.

[92] S. Emamian, B.B. Narakathu, A. Chlaihawi, B. Bazuin, and M.Z. Atashbar "Screen printing of flexible piezoelectric based device on polyethylene terephthalate (PET) and paper for touch and force sensing applications," Sensors & Actuators: A. Physical, vol. 263, pp. 639-647, 2017. DOI: 10.1016/j.sna.2017.07.045.

[93] D. A. Alsaid, E. Rebrosova, M. Joyce, M. Rebros, M. Atashbar and B. Bazuin, "Gravure printing of ITO transparent electrodes for applications in flexible electronics," Journal of Display Technology, vol. 8(7), pp. 391-396, 2012, doi: 10.1109/JDT.2012.2191765.

[94] S. Lim, M. Joyce, P. D. Fleming, A.T. Aijazi, M.Z. Atashbar, "Inkjet printing and sintering of nano-copper ink," Journal of Imaging Science and Technology, vol. 57(5), pp. 50506-1-50506-7, 7, 2013. DOI: 10.2352/J.ImagingSci.Technol.2013.57.5.050506.

[95] A. Moorthi, B. B. Narakathu, A. S. G. Reddy, A. Eshkeiti, M. Z. Atashbar, "A novel flexible strain gauge sensor fabricated using screen printing," the 6th International Conference on Sensing Technology: ICST, pp. 765-768, 2012. DOI: 10.1109/ICSensT.2012.6461780.

[96] S. Hajian, B. B. Narakathu, D. Maddipatla, S. Masihi, M. Panahi, R. G. Blair, B. J. Bazuin, M. Z. Atashbar, “Flexible temperature sensor based on fluorinated graphene,” IEEE EIT Conference, 2020, DOI: 10.1109/EIT48999.2020.9208256.

[97] S. Hajian, X. Zhang, D. Maddipatla, B. Baby Narakathu, J. I. Rodriguez-Labra, R. Blair, M. Z. Atashbar, “Flexible capacitive humidity sensor based on fluorinated graphene,” IEEE Sensors Conference, pp. 1-4, 2019. DOI: 10.1109/SENSORS43011.2019.8956564.

[98] V. Palaniappan, S. Masihi, X. Zhang, S. Emamian, A. K. Bose, D. Maddipatla, S. Hajian, M. Panahi, B. B. Narakathu, B. J. Bazuin, M. Z. Atashbar, “A flexible triboelectric nanogenerator fabricated using laser-assisted patterning process,” IEEE Sensors Conference, pp. 1-4, 2019. DOI: 10.1109/SENSORS43011.2019.8956682.

[99] S. Hajian, X. Zhang, D. Maddipatla, B. B. Narakathu, A. J. Hanson, R. G. Blair; M. Z. Atashbar, "Development of a fluorinated graphene-based flexible humidity sensor," IEEE International Conference on Flexible and Printable Sensors and Systems (FLEPS), pp. 1-3, 2019. DOI: 10.1109/FLEPS.2019.8792254

[100] A. K. Bose, X. Zhang, D. Maddipatla, S. Masihi, M. Panahi, B. B. Narakathu, B. J. Bazuin, M. Z. Atashbar, "Highly sensitive screen printed strain gauge for micro-strain detection," IEEE International Conference on Flexible and Printable Sensors and Systems (FLEPS), pp. 1-3, 2019. DOI:10.1109/FLEPS.2019.8792282

[101] X. Zhang, V. S. Turkani, S. Hajian, A. K. Bose, D. Maddipatla, A. J. Hanson, B. B. Narakathu, M. Z. Atashbar, "Novel printed carbon nanotubes based resistive humidity sensors," IEEE International Conference on Flexible and Printable Sensors and Systems (FLEPS), pp. 1-3, 2019. DOI:10.1109/FLEPS.2019.8792298.

[102] V. Palaniappan et al, "Laser-assisted fabrication of flexible micro-structured pressure sensor for low pressure applications," IEEE International Conference on Flexible and Printable Sensors and Systems (FLEPS), pp. 1-3, 2019. DOI:10.1109/FLEPS.2019.8792235

[103] D. Maddipatla, X. Zhang, A. K. Bose, S. Masihi, M. Panahi, V. Palaniappan, B. B. Narakathu, B. J. Bazuin, M. Z. Atashbar, "Development of a flexible force sensor using additive print manufacturing process," IEEE International Conference on Flexible and Printable Sensors and Systems (FLEPS), pp. 1-3, 2019. DOI: 10.1109/FLEPS.2019.8792307

[104] A. K. Bose, D. Maddipatla, B. B. Narakathu, B. J. Bazuin and M. Z. Atashbar, "Laser-assisted patterning of a flexible microplasma discharge device for heavy metal and salt detection in ambient air," IEEE International Conference on Flexible and Printable Sensors and Systems (FLEPS), pp. 1-3, 2019. DOI: 10.1109/FLEPS.2019.8792243

[105] D. Maddipatla, B.B. Narakathu, V.S. Turkani, S. Hajian, B.J. Bazuin, M.Z. Atashbar, “A flexible copper based electrochemical sensor using laser-assisted patterning process”, IEEE Sensors Conference, pp. 713-716, 2018, DOI: 10.1109/ICSENS.2018.8589754.

[106] V.S. Turkani, B.B. Narakathu, D. Maddipatla, B.N. Altay, P.D. Fleming B.J. Bazuin, M.Z. Atashbar, “Nickel based printed resistance temperature detector on flexible polyimide substrate”, IEEE Sensors Conference, pp. 356-359, 2018. DOI: 10.1109/ICSENS.2018.8589549.

[107] D. Maddipatla, B.B. Narakathu, V.S. Turkani, B.J. Bazuin, M.Z. Atashbar, “A gravure printed flexible electrochemical sensor for the detection of heavy metal compounds”, Eurosensors Conference, pp. 1201-1204, 2018, DOI: 10.3390/proceedings2130950.

[108] A.A. Chlaihawi, S. Emamian, B.B Narakathu, M.M Ali, D. Maddipatla, B.J. Bazuin, and M.Z. Atashbar, “A screen printed and flexible piezoelectric based AC magnetic field sensor” Sensors and Actuators, vol. 268, pp. 1-8, 2017.

[109] A. K. Bose, D. Maddipatla, B. B. Narakathu, V. S. Turkani, B. J. Bazuin, M. Z. Atashbar, “Flexible microplasma discharge device for the detection of biochemicals”, 17th International Meeting on Chemical Sensors (IMCS), pp. 419-420, 2018, DOI: 10.5162/IMCS2018/ME.4.

[110] D. Maddipatla, B. B. Narakathu, V. S. Turkani, B. J. Bazuin, M. Z. Atashbar, “Development of a gravure printed flexible electrochemical sensor”, 17th International Meeting on Chemical Sensors (IMCS), pp. 734-735, 2018, DOI: 10.5162/IMCS2018/P2EC.19.

[111] A.A. Chlaihawi, S. Emamian, B.B. Narakathu, B.J. Bazuin, M.Z. Atashbar, “Novel screen printed and flexible low frequency magneto-electric energy harvester”, 15th IEEE Sensors Conference, pp. 1622-1624, 2016. DOI: 10.1109/ICSENS.2016.7808947.

[112] D. Maddipatla, B.B. Narakathu, M.Z. Atashabar, “Recent progress in manufacturing techniques of printed and flexible sensors: A review”, Biosensors, vol. 10, pp. 199, 2020. DOI: 10.3390/bios10120199.

[113] A.A. Chlaihawi, S. Emamian, B.B. Narakathu, M.M. Ali, D. Maddipatla, B.J. Bazuin, M.Z. Atashbar, “Novel screen printed flexible magnetoelectric thin film sensor”, 30th Eurosensors Conference, pp. 1806-1809, 2016. DOI: 10.1016/j.proeng.2016.11.247.

[114] B. B. Narakathu, A. S. G. Reddy, D. Maddipatla, S. Emamian, A. Eshkeiti, A.A. Chlaihawi, B. J. Bazuin, M.Z. Atashbar, “Rapid prototyping of a flexible microfluidic sensing system using inkjet and screen printing processes”, 14th IEEE Sensors Conference, pp. 654-657, 2015. DOI: 10.1109/ICSENS.2015.7370340.

[115] S. Emamian, S.G.R. Avuthu, B.B. Narakathu, A. Eshkeiti, A. A. Chlaihawi, B.J. Bazuin, M.Z. Atashbar, “Fully printed and flexible piezoelectric based touch sensitive skin”, 14th IEEE Sensors Conference, pp. 1827-1830, 2015. DOI: 10.1109/ICSENS.2015.7370651.

[116] A. A. Chlaihawi, B.B. Narakathu, S. Emamian, A. Eshkeiti, S. G. R. Avuthu, B. J. Bazuin, M.Z. Atashbar, “Development of flexible dry ECG electrodes based on MWCNT/PDMS composite”, 14th IEEE Sensors Conference, pp. 221-224, 2015. DOI: 10.1109/ICSENS.2015.7370218.

[117] B.B. Narakathu, S.G.R. Avuthu, A. Eshkeiti, S. Emamian, M.Z. Atashbar, “Development of a novel printed flexible microfluidic sensing platform based on PCB technology”, Proceedings of IEEE Sensors Conference, pp. 665-668, 2014, DOI: 10.1109/ICSENS.2014.6985086.

[118] A. Eshkeiti, M.J. Joyce, B.B. Narakathu, S. Emamian, S.G.R. Avuthu, M. Joyce, M.Z. Atashbar, “A novel self-supported printed flexible strain sensor for monitoring body movement”, Proceedings of IEEE Sensors Conference, pp. 1615-1618, 2014. DOI: 10.1109/ICSENS.2014.6985328.

[119] A. Eshkeiti, S. Emamian, S.G.R. Avuthu, B.B. Narakathu, M.J. Joyce, M. Joyce, M.Z. Atashbar, “Screen printed flexible capacitive pressure sensor”, Proceedings of IEEE Sensors Conference, pp. 1192-1195, 2014. DOI: 10.1109/ICSENS.2014.6985222.

[120] B. B. Narakathu, S. G. A. Reddy, M. Z. Atashbar, E. Rebrosova, M. Rebros, M. K. Joyce, “A novel gravure printed impedance based flexible electrochemical sensor”, Proceedings of IEEE Sensors Conference, pp. 577-580, 2011. DOI: 10.1109/ICSENS.2011.6127225.

[121] S. Hajian et al., “Humidity sensing properties of halogenated graphene: A comparison of fluorinated graphene and chlorinated graphene”, IEEE International Conference on Flexible

and Printable Sensors and Systems (FLEPS), pp. 1-4, 2020. DOI: 10.1109/FLEPS49123.2020.9239564.

[122] D. Maddipatla, X. Zhang, A.K. Bose, S. Masihi, B.B. Narakathu, B.J. Bazuin, M.Z. Atashbar, “A polyimide based force sensor fabricated using additive screen-printing process for flexible electronics”, IEEE Access, vol. 8, pp. 207813 – 207821, 2020.

[123] X. Zhang et al., “Printed carbon nanotubes-based flexible resistive humidity sensor”, IEEE Sensors Journal, vol. 20(21), pp. 12592-12601, 2020, doi: 10.1109/JSEN.2020.3002951.

[124] A. Eshkeiti et al, “Screen printing of multi-layered hybrid printed circuit boards on different substrates,” IEEE Transactions on Device and Materials Reliability, vol. 5(3), pp. 415-421, 2015.

[125] A. Eshkeiti, “A novel inkjet printed surface enhanced raman spectroscopy (SERS) substrate for the detection of toxic heavy metals,” Procedia Eng., vol. 25, pp. 338–341, 2011.

[126] M. J. Joyce, A. Eshkeiti, P. D. Fleming III, A. Pekarovicova, M. Z. Atashbar, “Self supported printed multi-layer capacitor,” Journal of Print and Media Technology Research, vol.4(1), pp. 285-300, 2015.

[127] H. Zhu, B. B Narakathu, Z. Fang, A. T. Aijazi, M. Joyce, M. Z. Atashbarbr, L. Hu,“A gravure printed antenna on shape-stable transparent nanopaper,” Nanoscale, vol. 6, pp. 9110-9115, 2014.

[128] J. Fraden, “Handbook of modern sensors: physics, designs, and applications,” Springer, pp. 2, 2004.

[129] S. Choi et al. “Recent advances in flexible and stretchable bio-electronic devices integrated with nanomaterials,” Adv. Mater., vol. 28(22), pp. 4203-4218, 2016.

[130] D.E. Leber et al. “Advances in flexible hybrid electronics reliability,” In 2017 IEEE Workshop on Microelectronics and Electron Devices (WMED), IEEE, pp. 1-4, 2017.

[131] Y. Ma et al. “Flexible hybrid electronics for digital healthcare,” Adv. Mater. Vol. 32(15), pp. 1902062, 2020.

[132] Flexible Hybrid Electronics: New IDTechEx Report on Innovation Trends, Opportunities and Challenges. Accessed July 11, 2021. https://agilitypr.news/Flexible-Hybrid-Electronics-New-IDTechE-9650.

[133] T. Liang, Y. J. Yuan, “Wearable medical monitoring ystems based on wireless networks: A review,” IEEE Sensors Journal, 16(23), 8186–8199, 2016.

[134] D.S. Beaudoin and S.O. Obare, “Dual optical and electrochemical glucose detection based on a dipyridophenazine ligand,” Tetrahedron Lett., vol. 49, pp. 6054-6057, 2008.

[135] A. Yildirim, R. Rahimi, S. S. Es-haghi, A. Vadlamani, F. Peng, M. Oscai, and M. Cakma, “Roll-to-Roll (R2R) production of ultrasensitive, flexible, and transparent pressure sensors based on vertically aligned lead zirconate titanate and graphene nanoplatelets,” Adv.Mater. Technol., vol. 4 (3), pp. 1800425, 2019.

[136] Y. Yang et al. “Flexible piezoelectric pressure sensor based on polydopamine-modified BaTiO3/PVDF composite film for human motion monitoring,” Sensors and Actuators A: Physical, vol. 301 pp. 111789, 2020.

[137] X. Lin et al. “Flexible piezoresistive sensors based on conducting polymer-coated fabric applied to human physiological signals monitoring,” Journal of Bionic Engineering, vol. 17(1), pp. 55-63, 2020.

[138] N. Luo et al, “Flexible piezoresistive sensor patch enabling ultralow power cuffless blood pressure measurement,” Adv. Funct. Mater., vol. 26(8), pp. 1178-1187, 2016.

[139] H. Kim, G. Kim, T. Kim, S. Lee, et al, “Transparent, flexible, conformal capacitive pressure sensors with nanoparticles,” Small, vol.14(8), pp. 1703432, 2018.

[140] H. Vandeparre, D. Watson, and S. P. Lacour, “Extremely robust and conformable capacitive pressure sensors based on flexible polyurethane foams and stretchable metallization,” Applied Physics Letters, vol. 103(20), pp. 204103, 2014.

[141] V. Mitrakos et al. “Design, manufacture and testing of capacitive pressure sensors for low-pressure measurement ranges,” Micromachines, vol. 8(2), pp. 41, 2017.

[142] S. Masihi, M. Panahi et al, “Highly sensitive porous PDMS-based capacitive pressure sensors fabricated on fabric platform for wearable applications,” ACS Sens, 6, 3, 938–949, 2021.

[143] L. Dana, S. Shia, H. J. Chunga, and A. Elias, “Porous polydimethylsiloxane−silver nanowire devices for wearable pressure sensors,” ACS Appl. Nano Mater. 2019, 2, 4869−4878.

[144] J. C. Yang et al, “Microstructured porous pyramid-based ultrahigh sensitive pressure sensor insensitive to strain and temperature,” ACS Appl. Mater. Interfaces, 11, 21, 19472–19480, 2019.

[145] J. Hwang et al, “Abrication of hierarchically porous structured PDMS composites and their application as a flexible capacitive pressure sensor,” Composites Part B: Engineering, vol. 211, 108607, 2021.

[146] S. Jang and J. Hoon Oh, “Rapid fabrication of microporous BaTiO3/PDMS nanocomposites for triboelectric nanogenerators through one-step microwave irradiation,” Scientific REPORTS, vol. 2018, p.14287, 2018.

[147] P. Wei, X. Guo, X. Qiu and D. Yu, “Flexible capacitive pressure sensor with sensitivity and linear measuring range enhanced based on porous composite of carbon conductive paste and polydimethylsiloxane,” Nanotechnology, vol. 30, p.455501, 2019.

[148] S. Peng, S. Chen, Y. Haung, S. Pei, X. Guo, “High sensitivity capacitive pressure sensor with bi-layer porous structure elastomeric dielectric formed by a facile solution based process, ” IEEE Sensors Letters, vol. 3 (2), p. 2500104, Feb. 2019.

[149] J. Oh et al., “Highly uniform and low hysteresis piezoresistive pressure sensors based on chemical grafting of Polypyrrole on elastomer template with uniform pore size,” Small, 2019, 15, 1901744.

[150] C. Gerlach et al “Printed MWCNT-PDMS-composite pressure sensor system for plantar pressure monitoring in ulcer prevention,” J. IEEE Sens., vol. 15(7), pp 3647-3656, 2015.

[151] A. Rinaldi, A. Tamburrano, M. Fortunato and M. S. Sarto, “A flexible and highly sensitive pressure sensor based on a PDMS foam coated with graphene nanoplatelets,” Sensors, vol. 16 (12), pp.2148, 2016.

[152] D. Maddipatla, B. B. Narakathu, M. M. Ali, A. A. Chlaihawi and M. Z. Atashbar, “Development of a novel carbon nanotube based printed and flexible pressure sensor,” IEEE Sens., pp. 1-4, 2017, doi: 10.1109/SAS.2017.7894034.

[153] H.S. Jahromi, A. Setoodeh, “Longitudinal, transverse, and torsional free vibrational and mechanical behavior of silicon nanotubes using an atomistic model,” Materials Research, 23(2): e20200075, 2020.

[154] H. Ding et al, “Influence of the pore size on the sensitivity of flexible and wearable pressure sensors based on porous Ecoflex dielectric layers,” Mate. Res. Express, vol.36 (6),pp. 2-7 , 2019.

[155] S. W. Park, P.S. Das, A. Chhetry, and J. Y. Park, “A flexible capacitive pressure sensor for wearable respiration monitoring system,” IEEE Sens Journal, vol. 17 (20), pp. 6558 – 6564, 2017.

[156] O. Atalay, A. Atalay, J. Gafford, and C. Walsh, “A highly sensitive capacitive-based soft pressure sensor based on a conductive fabric and a microporous dielectric layer,” Adv. Mater. Technol., vol. 3 (1), pp. 1700237, 2018.

[157] J. Oh et al, “Highly uniform and low hysteresis piezoresistive pressure sensors based on chemical grafting of polypyrrole on elastomer template with uniform pore size,” Small, vol. 15 , p. 1901744, 2019.

[158] B.B. Narakathu et. al., “A novel fully printed and flexible capacitive pressure sensor,” IEEE Sens. Proc., pp. 1935-1938, 2012.

[159] Y. Zang, F. Zhang, C.A. Di, D. Zhu, “Advances of flexible pressure sensors toward artificial intelligence and health care applications,” Mate. Horiz., vol. 2, pp. 140-156, 2015.

[160] T. Kameya, Y. Matsuda, Y. Egami, H. Yamaguchi, T. Niimi, “Dual luminescent arrays sensor fabricated by inkjet-printing of pressure-and temperature-sensitive paints,” Sens. Actuators, B, vol. 190, pp. 70-77, 2014.

[161] M. Holmer, F. Sandberg, K.Solem, E. Grigonyt˙e, B. Oldeand, and L. S¨ornmo, “Extracting a cardiac signal from the extracorporeal pressure sensors of a hemodialysis machin,” IEEE Trans. Biomed. Eng., vol. 62 (5), pp. 1305-1314, 2015.

[162] Juha M. Kortelainen, and J. Virkkala, “FFT averaging of multichannel BCG signals from bed mattress sensor to improve estimation of heart beat interval, ” Int. Conf. of the IEEE EMBS, pp. 6685, 2007.

[163] P. G, Jung, G. Lim, S. Kim, and K. Kong, “A wearable gesture recognition device for detecting muscular activities based on air-pressure sensors,” IEEE Trans. Ind. Informat, Vol. 11 (2), pp. 485-494, 2015.

[164] V Palaniappan, S Masihi, M Panahi, D Maddipatla, X Zhang, BB Narakathu, BJ Bazuin, MZ Atashbar, “A porous microstructured dielectric layer based pressure sensor for wearable applications,” 2021 IEEE International Conference on Flexible and Printable Sensors and Systems (FLEPS), pp. 1-4, 2021, DOI: 10.1109/FLEPS51544.2021.9469706.

[165] Normal Respiratory Frequency, Volume, Chart. Accessed July 12, 2021. https://www.normalbreathing.com/respiratory-rate-volume-chart.